AGU PUBLICATIONS

Paleoceanography

RESEARCH ARTICLE
10.1002/2016PA003003

Key Points:
- The West Greenland surface sediments were quality-checked regarding "modern" age using radionuclide measurements
- Sea ice and sea surface temperature (SST) transfer functions were developed from the modern diatom data set
- April Sea Ice Concentration and July SST were reconstructed in Disko Bay for the past circa 11000 years

Supporting Information:
- Table S1
- Table S2

Correspondence to:
D. W. Krawczyk,
dikr@natur.gl

Citation:
Krawczyk, D. W., A. Witkowski, M. Moros, J. M. Lloyd, J. L. Høyer, A. Miettinen, and A. Kuijpers (2017), Quantitative reconstruction of Holocene sea ice and sea surface temperature off West Greenland from the first regional diatom data set, *Paleoceanography*, *32*, 18–40, doi:10.1002/2016PA003003.

Received 12 JUL 2016
Accepted 13 DEC 2016
Accepted article online 15 DEC 2016
Published online 8 JAN 2017

Quantitative reconstruction of Holocene sea ice and sea surface temperature off West Greenland from the first regional diatom data set

D. W. Krawczyk[1], A. Witkowski[2,3], M. Moros[4], J. M. Lloyd[5], J. L. Høyer[6], A. Miettinen[7], and A. Kuijpers[8]

[1]Greenland Climate Research Centre, Greenland Institute of Natural Resources, Nuuk, Greenland, [2]Palaeoceanology Unit, Faculty of Geosciences, University of Szczecin, Szczecin, Poland, [3]Natural Sciences Education and Research Centre, University of Szczecin, Szczecin, Poland, [4]Leibniz Institute for Baltic Sea Research Warnemünde, Rostock, Germany, [5]Department of Geography, University of Durham, Durham, UK, [6]Danish Meteorological Institute, Copenhagen Oe, Denmark, [7]Norwegian Polar Institute, Fram Centre, Tromsø, Norway, [8]Geological Survey of Denmark and Greenland, Copenhagen K, Denmark

Abstract Holocene oceanographic conditions in Disko Bay, West Greenland, were reconstructed from high-resolution diatom records derived from two marine sediment cores. A modern data set composed of 35 dated surface sediment samples collected along the West Greenland coast accompanied by remote sensing data was used to develop a diatom transfer function to reconstruct April sea ice concentration (SIC) supported by July sea surface temperature (SST) in the area. Our quantitative reconstruction shows that oceanographic changes recorded throughout the last ~11,000 years reflect seasonal interplay between spring (April SIC) and summer (July SST) conditions. Our records show clear correlation with climate patterns identified from ice core data from GISP2 and Agassiz-Renland for the early to middle Holocene. The early Holocene deglaciation of western Greenland Ice Sheet was characterized in Disko Bay by initial strong centennial-scale fluctuations in April SIC with amplitude of over 40%, followed by high April SIC and July SST. These conditions correspond to a general warming of the climate in the Northern Hemisphere. A decrease in April SIC and July SST was recorded during the Holocene Thermal Optimum reflecting more stable spring-summer conditions in Disko Bay. During the late Holocene, high April SIC characterized the Medieval Climate Anomaly, while high July SST prevailed during the Little Ice Age, supporting previously identified antiphase relationship between surface waters in West Greenland and climate in NW Europe. This antiphase pattern might reflect seasonal variations in regional oceanographic conditions and large-scale fluctuations within the North Atlantic Oscillation and Atlantic Meridional Overturning Circulation.

1. Introduction

Diatoms are a common and abundant component of Arctic phytoplankton communities, and their distribution is strongly influenced by sea ice cover and surface water temperature [*Hasle and Syvertsen*, 1996; *Quillfeldt*, 2001; *Arrigo et al.*, 2012]. Melting sea ice and glacial discharge along the coasts of Greenland influence succession and distribution of the marine diatoms [e.g., *Gradinger and Baumann*, 1991; *Quillfeldt*, 1996, 2001]. Diatom blooms in particular tend to follow the receding sea ice edge during summer with changing species composition over the growth season [*Gradinger and Baumann*, 1991]. Diatom species belonging to genera, such as *Fragilariopsis*, *Thalassiosira*, and *Chaetoceros* are common in coastal waters of Greenland, Svalbard, Iceland, and Norway during spring and summer blooms [e.g., *Hasle and Syvertsen*, 1996; *Hasle and Heimdal*, 1998; *Quillfeldt*, 2001; *Jensen*, 2003; *Degerlund and Eilertsen*, 2010; *Krawczyk et al.*, 2015]. These diatom genera are also common in adjacent marine sediments and have been successfully used in reconstructing the past environments. In the North Atlantic region diatoms have been used as a tool for reconstructing quantitative sea ice concentration (SIC) and sea surface temperature (SST) throughout the Holocene using transfer function method [e.g., *Jiang et al.*, 2001; *Andersen et al.*, 2004a, 2004b; *Justwan and Koç*, 2008; *Berner et al.*, 2011; *Miettinen et al.*, 2012, 2015]. However, diatom-based reconstructions along West Greenland have so far primarily been qualitative [e.g., *Jensen*, 2003; *Moros et al.*, 2006; *Ren et al.*, 2009; *Krawczyk et al.*, 2010, 2013]. An exception to this is a recent transfer function study by *Sha et al.* [2014] using a modern data set collected mostly from coastal waters around Iceland and some off Greenland (expanded from *Jiang et al.* [2001]).

Millennial-scale climate fluctuations during the last 10,000 years have been identified in the Greenland-Arctic region [*O'Brien et al.*, 1995; *Alley et al.*, 1999] and in the North Atlantic region [*Andersen et al.*, 2004a, 2004b; *Miettinen et al.*, 2012]. These fluctuations are generally linked to shifts in sea ice cover and Greenland Ice Sheet extent, the North Atlantic Current system, the North Atlantic Oscillation (NAO), and the Atlantic Meridional Overturning Circulation (AMOC). Fluctuations in sea ice cover, NAO, and AMOC are also suggested to explain a recently identified late Holocene antiphase relationship between West Greenland surface water temperatures and northwest European climate, resembling the present-day climate seesaw [e.g., *Seidenkrantz et al.*, 2007, 2008; *Krawczyk et al.*, 2013]. *Bianchi* and *McCave* [1999] suggested Holocene climate variability at ~2500, ~1500, and ~950 years periodicities, possibly caused by changes in solar flux and internal oscillation of the climate system. During the last millennium, a pronounced climatic cooling has been widely recognized in the Northern Hemisphere [e.g., *Kaufman et al.*, 2009; *Vinther et al.*, 2009; *McGregor et al.*, 2015]. However, recent studies show a warm anomaly in surface waters of West Greenland and subpolar North Atlantic during the Little Ice Age [*Seidenkrantz et al.*, 2008; *Miettinen et al.*, 2012; *Krawczyk et al.*, 2013]. Over the past few decades a tendency toward increased water temperature and reduced sea ice cover in the Baffin Bay and Arctic Ocean [*Comiso*, 2006] as well as increased freshwater runoff from the Greenland Ice Sheet [*Hanna et al.*, 2008; *Vinther et al.*, 2009] have been observed. Also, an extreme phase during the winter NAO phase has been revealed, contributing to the wintertime warming across Europe and cooling conditions in the NW Atlantic [*Hurrel*, 1995]. Nevertheless, the dynamics of the ocean-climate system are still poorly understood and a better understanding of the relationship between ocean and climate on a longer timescale is necessary to help estimate future climate changes.

This paper presents high-resolution quantitative reconstructions of primarily SIC supported by SST for the outer Disko Bay, West Greenland region using diatom transfer functions for the past ~11,000 years. We have investigated the Holocene oceanographic changes based on a newly developed modern diatom data set collected from the West Greenland coast between 59°N and 72°N. The purpose of this paper is to present the identified seasonal variability in SIC along with SST in the context of regional and large-scale oscillations within the ocean-climate system in the Arctic during the Holocene.

2. Oceanographic Setting

Baffin Bay is located within Arctic climate zone with average air temperature in July below 10°C and surface water temperature of ~5°C [*Boertmann et al.*, 2013]. The oceanography along the West Greenland shelf is governed by the seasonal sea ice cover, West Greenland Current (WGC; Figure 1) and glacial ice originating from the Greenland Ice Sheet. In winter and spring, two types of sea ice occur in the Baffin Bay region, i.e., drift ice ("West Ice") and fast ice anchored to the coast [*Boertmann et al.*, 2013]. Sea ice starts to form in northern Baffin Bay at the end of September and covers much of the area by late December. Maximum sea ice extent is observed in March–April, leaving area south of Fyllas Banke largely ice free [*Boertmann et al.*, 2013; *Juul-Pedersen et al.*, 2014]. In contrast, minimum sea ice cover in Baffin Bay along with higher water temperatures appear from June/July to September (e.g., Figure 2) [*Boertmann and Mosbech*, 2011; *Juul-Pedersen et al.*, 2014; *Ribergaard*, 2014]. The WGC is composed of cold, low-salinity Polar Water (PW) of Arctic origin and the temperate, saline Irminger Water (IW) of Atlantic origin [*Buch*, 1981; *Tang et al.*, 2004; *Ribergaard*, 2014] (Figure 1). The IW can be traced all along the coast [*Buch* 1990] and on average has a temperature of 3.5–4.5°C and salinity of 34.2–34.9 [*Buch*, 1981; *Lloyd*, 2006; *Ribergaard*, 2014]. The PW has a temperature from 1–2°C in SW Greenland to −1°C in the Uummannaq area with salinity below 33.7 [*Ribergaard*, 2014]. The PW loses its momentum around the latitude of Fyllas Banke and does not penetrate northern Baffin Bay [*Boertmann and Mosbech*, 2011; *Boertmann et al.*, 2013] allowing the IW to rise toward the surface. The WGC flows northward through Disko Bay and Vaigat Strait (Figure 1) and is influenced by meltwater from sea ice and glacial discharge from fjords and outlet glaciers on its way north [*Boertmann et al.*, 2013]. The complex topography of the West Greenland shelf and the strong tidal currents deflect the WGC around the shallow banks [*Ribergaard et al.*, 2004; *Söderkvist et al.*, 2006].

Sedimentation along the West Greenland shelf varies significantly between coastal and offshore regions, as well as northern and southern regions and is not well established. In previous studies, high sedimentation rates were recorded in near-shore Disko Bay and Vaigat Strait (~0.5–1 mm/yr) [*Perner et al.*, 2013; *Moros*

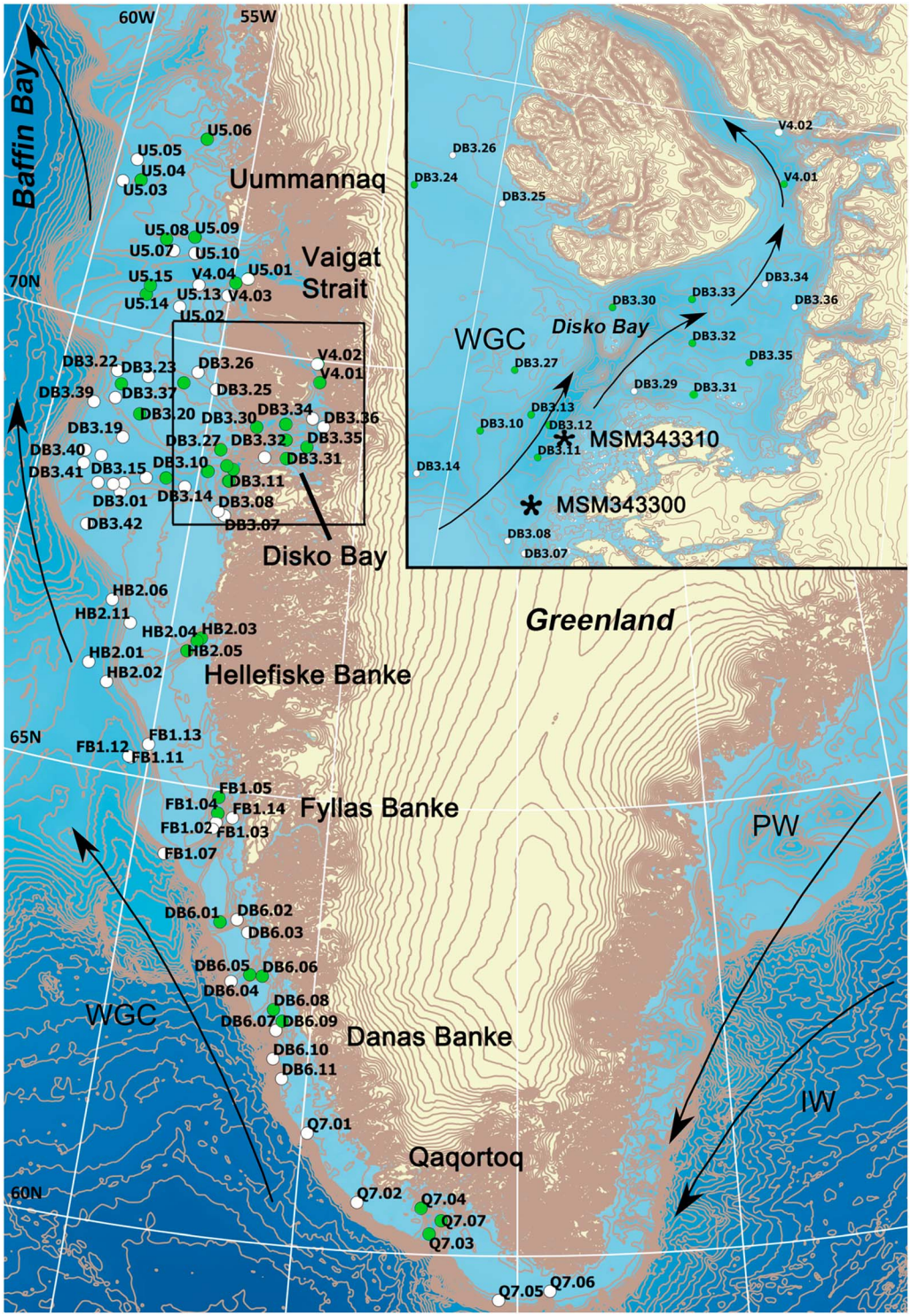

Figure 1. Location map of the West Greenland shelf showing positions of the sampling stations (green and white circles) with marked samples regarded as modern (green circles). Names of the sampled regions are given on the map (for more details see Table 1). The gravity cores were collected from Disko Bay, i.e. MSM343310 and MSM343300 (solid stars in insert map). A schematic circulation system around Greenland is also shown, i.e. WGC—West Greenland Current with source waters, i.e., IW—Irminger Water and PW—Polar Water.

Table 1. List of Sampled Stations (Surface Sediments and Sediment Cores) With Information on Their Geographic Positions, Water Depths, Sampling Equipment, Lithological Description, and Isotope Dating[a]

Station	Region	Latitude N	Longitude W	Water Depth (m)	Equipment	Lithological Description	$^{210}Pb_{unsupp.}$ (^{137}Cs) Bq/kg
				Surface Sediments			
Q7.01	Qaqortoq	61°16.2	49°52.3	440	Box corer	grey clay with sand/gravel	2 ± 7 (/)
Q7.02	Qaqortoq	60°32.2	48°37.3	331	Box corer	olive green sandy, silty mud	16 ± 7 (/)
Q7.03	Qaqortoq	60°13.7	46°58.2	455	Box corer	olive green sandy, silty mud	190 ± 10 (5.4 ± 0.5)
Q7.04	Qaqortoq	60°30.3	47°10	412	Box corer	olive green mud	249 ± 17 (5.8 ± 1.3)
Q7.05	Qaqortoq	59°30.7	45°24.7	338	Box corer	olive green greyish silty mud	79 ± 13 (5.8 ± 0.7)
Q7.06	Qaqortoq	59°36.4	44°17.1	349	Box corer	olive green silty mud, stones	/
Q7.07	Qaqortoq	60°22.6	46°42.4	508	Box corer	olive green mud	240 ± 8 (5.1 ± 0.6)
DB6.01	Danas Banke	63°31	52°30.4	364	Grab	olive green mud	153 ± 9 (1.2 ± 0.4)
DB6.02	Danas Banke	63°34	52°05.6	456	Grab	olive green mud with some sand	88 ± 7 (/)
DB6.03	Danas Banke	63°26.5	51°46.9	386	Grab	olive green mud with some sand	34 ± 7 (/)
DB6.04	Danas Banke	62°52.4	52°02.9	350	Grab	olive green sandy mud, stones	106 ± 10 (/)
DB6.05	Danas Banke	62°58.1	51°36.3	503	Grab	olive green greyish mud	298 ± 14 (10.5 ± 1.1)
DB6.06	Danas Banke	62°58.4	51°18.2	463	Grab	olive dark green mud	240 ± 13 (8.1 ± 1.0)
DB6.07	Danas Banke	62°23	50°49.9	520	Box corer	olive green sandy mud	23 ± 5 (1.4 ± 0.3)
DB6.08	Danas Banke	62°36.5	50°56.6	394	Grab	olive green greyish mud	288 ± 13 (4.1 ± 0.6)
DB6.09	Danas Banke	62°29.6	50°42.1	384	Grab	olive green greyish mud	444 ± 14 (3.3 ± 0.9)
DB6.10	Danas Banke	62°03.7	50°49.8	954	Grab	olive green sandy, silty mud	/
DB6.11	Danas Banke	61°51	50°34.9	304	Grab	muddy sand	/
FB1.02	Fyllas Banke	64°33.3	53°00.3	420	Box corer	olive green mud	95 ± 7 (1.1 ± 0.3)
FB1.03	Fyllas Banke	64°37.1	52°57.1	543	Box corer	olive green mud, stones	/
FB1.04	Fyllas Banke	64°43.6	52°56.6	533	Box corer	olive green mud	/
FB1.05	Fyllas Banke	64°54.8	52°58.3	430	Box corer	olive green mud	255 ± 15 (3.1 ± 1.1)
FB1.07	Fyllas Banke	64°11.6	54°10.2	620	Box corer	olive green mud with sand	14 ± 7 (/)
FB1.11	Fyllas Banke	65°11.8	55°27.6	809	Box corer	olive green mud	27 ± 8 (/)
FB1.12	Fyllas Banke	65°12.7	55°32	780	Box corer	olive green mud, stones	80 ± 8 (/)
FB1.13	Fyllas Banke	65°22.8	55°03.5	393	Grab	sand with some olive green mud, stones	48 ± 4 (/)
FB1.14	Fyllas Banke	64°41.7	52°32.4	418	Grab	olive green mud	/
HB2.01	Hellefiske Banke	66°10.4	57°07.3	672	Box corer	olive green mud	118 ± 7 (1.1 ± 0.3)
HB2.02	Hellefiske Banke	65°59.6	56°30.9	589	Box corer	olive green mud, stones	11 ± 8 (/)
HB2.03	Hellefiske Banke	66°40.4	54°05.8	463	Box corer	olive green mud	/
HB2.04	Hellefiske Banke	66°37.5	54°12.8	410	Box corer	olive green and black mud	316 ± 11 (1.1 ± 0.5)
HB2.05	Hellefiske Banke	66°29.7	54°27.2	430	Box corer	olive green and black mud	307 ± 10 (1.0 ± 0.5)
HB2.06	Hellefiske Banke	66°55.2	56°49.6	647	Box corer	olive green mud with sand	99 ± 7 (/)
HB2.11	Hellefiske Banke	66°41.8	56°11.4	175	Grab	sand with some olive green mud	/
DB3.01	Disko Bay	68°08.4	57°16.1	342	Box corer	olive green mud with sand, stones	126 ± 6 (0.5 ± 0.3)
DB3.02	Disko Bay	68°15	57°12.3	405	Box corer	olive green mud	61 ± 6 (/)
DB3.03	Disko Bay	68°12.6	57°32	426	Box corer	olive green mud	60 ± 9 (/)
DB3.04	Disko Bay	68°11.1	58°00	424	Box corer	olive green mud	/
DB3.07	Disko Bay	68°05.5	54°00	145	Box corer	olive grey silty clay	/
DB3.08	Disko Bay	68°07.7	54°12.4	357	Box corer	olive green mud with sand, stones	6 ± 4(/)
DB3.10	Disko Bay	68°33.8	54°43.2	293	Grab	olive green mud	210 ± 8(0.5 ± 0.3)
DB3.11	Disko Bay	68°29.5	54°01.3	575	Grab	olive brown mud	218 ± 11 (0.7 ± 0.2)
DB3.12	Disko Bay	68°37.5	53°56.9	678	Grab	olive green and black mud	570 ± 13 (2.3 ± 0.7)
DB3.13	Disko Bay	68°39.3	54°09.9	486	Grab	olive green mud	309 ± 9 (1.1 ± 0.5)
DB3.14	Disko Bay	68°20.1	55°20.7	532	Grab	olive green mud	138 ± 16 (/)
DB3.15	Disko Bay	68°21.3	56°34.5	482	Grab	olive green brownish mud	134 ± 8 (/)
DB3.16	Disko Bay	68°24.2	55°57.9	539	Grab	olive green brownish mud	250 ± 20 (3.5 ± 1.2)
DB3.18	Disko Bay	68°29.8	58°05.4	316	Grab	olive green mud	/
DB3.19	Disko Bay	68°45.6	57°33.7	308	Grab	olive green mud	/
DB3.20	Disko Bay	69°03.6	57°11.5	219	Grab	olive green mud	135 ± 10 (0.7 ± 0.3)
DB3.22	Disko Bay	69°29.5	58°11.8	288	Grab	olive green mud	43 ± 6 (/)
DB3.23	Disko Bay	69°30	57°10	211	Grab	olive green mud	120 ± 9 (/)
DB3.24	Disko Bay	69°30.4	55°59.4	231	Grab	olive green brownish mud	130 ± 8 (0.5 ± 0.3)
DB3.25	Disko Bay	69°30	54°54.7	161	Grab	olive green sandy mud	78 ± 6 (/)
DB3.26	Disko Bay	69°39.4	55°35.8	160	Grab	olive green sandy mud	61 ± 5 (/)
DB3.27	Disko Bay	68°49.7	54°26.4	188	Grab	olive green mud	146 ± 6 (1.1 ± 0.4)
DB3.29	Disko Bay	68°48.9	53°01.5	716	Grab	olive green and black mud	/

Table 1. (continued)

Station	Region	Latitude N	Longitude W	Water Depth (m)	Equipment	Lithological Description	$^{210}Pb_{unsupp.}$ (^{137}Cs) Bq/kg
DB3.30	Disko Bay	69°08.9	53°25.2	347	Grab	olive green sandy mud with stones	156 ± 11 (/)
DB3.31	Disko Bay	68°50.1	52°20.2	281	Grab	olive green mud	199 ± 13 (/)
DB3.32	Disko Bay	69°02.9	52°25.7	300	Grab	olive light green mud with sand	198 ± 11 (2.1 ± 0.5)
DB3.33	Disko Bay	69°13.9	52°30.2	505	Grab	olive green mud	245 ± 13(2.4 ± 0.5)
DB3.34	Disko Bay	69°20	51°39.3	327	Grab	olive green grey mud	84 ± 14 (/)
DB3.35	Disko Bay	68°59.8	51°44.1	327	Grab	olive green mud	181 ± 13 (/)
DB3.36	Disko Bay	69°14.9	51°17	367	Grab	olive light green silty mud	144 ± 8 (/)
DB3.37	Disko Bay	69°21.2	57°58.9	287	Grab	olive green brown mud	223 ± 9 (1.6 ± 0.6)
DB3.38	Disko Bay	69°11	58°03.9	273	Grab	olive green sandy mud	/
DB3.39	Disko Bay	69°04.8	58°42.6	404	Grab	olive brown mud with sand	48 ± 5 (/)
DB3.40	Disko Bay	68°31.2	58°37.1	320	Grab	olive green sandy mud	/
DB3.41	Disko Bay	68°22.3	58°34.2	342	Grab	olive green sandy mud	/
DB3.42	Disko Bay	67°42.1	58°02.7	282	Grab	olive green sandy mud	99 ± 6 (1.2 ± 0.4)
V4.01	Vaigat Strait	69°45.1	51°33.9	466	Grab	olive brown silty mud	152 ± 14 (1.4 ± 0.5)
V4.02	Vaigat Strait	69°57.5	51°42.8	381	Grab	olive green brownish silty mud	130 ± 12 (1.2 ± 0.6)
V4.03	Vaigat Strait	70°35.1	55°03.9	322	Grab	olive dark green sandy and silty mud	131 ± 7 (/)
V4.04	Vaigat Strait	70°44.8	54°52.6	522	Box corer	olive dark green silty mud	172 ± 9 (0.5 ± 0.2)
U5.01	Uummannaq	70°49.3	54°28.5	555	Grab	olive green silty mud	72 ± 7 (1.2 ± 0.3)
U5.02	Uummannaq	70°21.7	56°37.8	249	Grab	olive green sandy mud	/
U5.03	Uummannaq	71°37.7	59°35.8	445	Grab	olive grey silty mud	/
U5.04	Uummannaq	71°41.3	58°57.8	366	Grab	olive brown silty mud	146 ± 10 (1.1 ± 0.6)
U5.05	Uummannaq	71°54.5	59°16.9	413	Grab	brownish grey silty mud	69 ± 7 (0.5 ± 0.2)
U5.06	Uummannaq	72°19.4	56°53.4	350	Grab	olive grey silty mud	/
U5.07	Uummannaq	70°58.9	57°14.2	344	Grab	olive green mud	/
U5.08	Uummannaq	71°05.5	57°34.1	322	Box corer	olive light green mud	150 ± 7 (2.6 ± 0.6)
U5.09	Uummannaq	71°11	56°35.7	293	Grab	olive green brown mud	152 ± 7 (0.7 ± 0.2)
U5.10	Uummannaq	71°00	56°28.6	387	Grab	olive green grey silty mud	147 ± 19 (/)
U5.13	Uummannaq	70°39.1	56°07.5	485	Grab	olive green silty mud	/
U5.14	Uummannaq	70°25	57°50.5	421	Grab	olive light green sandy and silty mud	190 ± 8 (0.9 ± 0.3)
U5.15	Uummannaq	70°31.6	57°46.4	455	Grab	olive green brown mud	189 ± 7 (1.9 ± 0.3)
				Sediment Cores			
MSM300	Disko Bay	68°28.3	54°00.1	519	Gravity corer	*Harff et al.* [2016]	
MSM310	Disko Bay	68°38.8	53°49.4	855	Gravity corer	*Harff et al.* [2016]	

[a]Samples regarded as modern and included in statistical analysis are presented in underline.

et al., 2016], while low sedimentation rate is observed from offshore SW Greenland (~0.25 mm/yr) [*Seidenkrantz et al.*, 2013].

3. Materials and Methods

3.1. Environmental Variables

The modern environmental data used in this study, i.e., sea ice concentration (SIC) and sea surface temperature (SST), were obtained from satellite reanalysis (see example given in Figure 2). The SST reanalysis data were constructed from 1982 to 2012 using infrared satellite observations from the Pathfinder 5.2 project [*Casey et al.*, 2010] and the Along Track Scanning Radiometer Reprocessing for Climate data set [*Embury and Merchant*., 2012]. The two data sets were interpolated as described in *Høyer* and *She* [2007] using the bias correction method presented in *Høyer et al.* [2014] to produce daily gap free SST fields with a spatial resolution of 0.05° latitude and longitude. SST fields from year 2013 and 2014 were taken from the operational runs. Validation against independent in situ observations has shown that the daily SST fields have an uncertainty of 0.5°C. Average monthly SST fields were constructed from the daily time series and the SST values from the grid point covering the positions of the surface sediment stations (see Figure 1 and Table 1 for exact location) were extracted. Similarly, the SIC fields were obtained from monthly averages of the Ocean and Sea Ice Satellite Application Facility climate data record. The data set is constructed from passive microwave satellite observations [see, e.g., *Andersen et al.*, 2007] and is delivered on a 10 km spatial resolution stereopolar grid

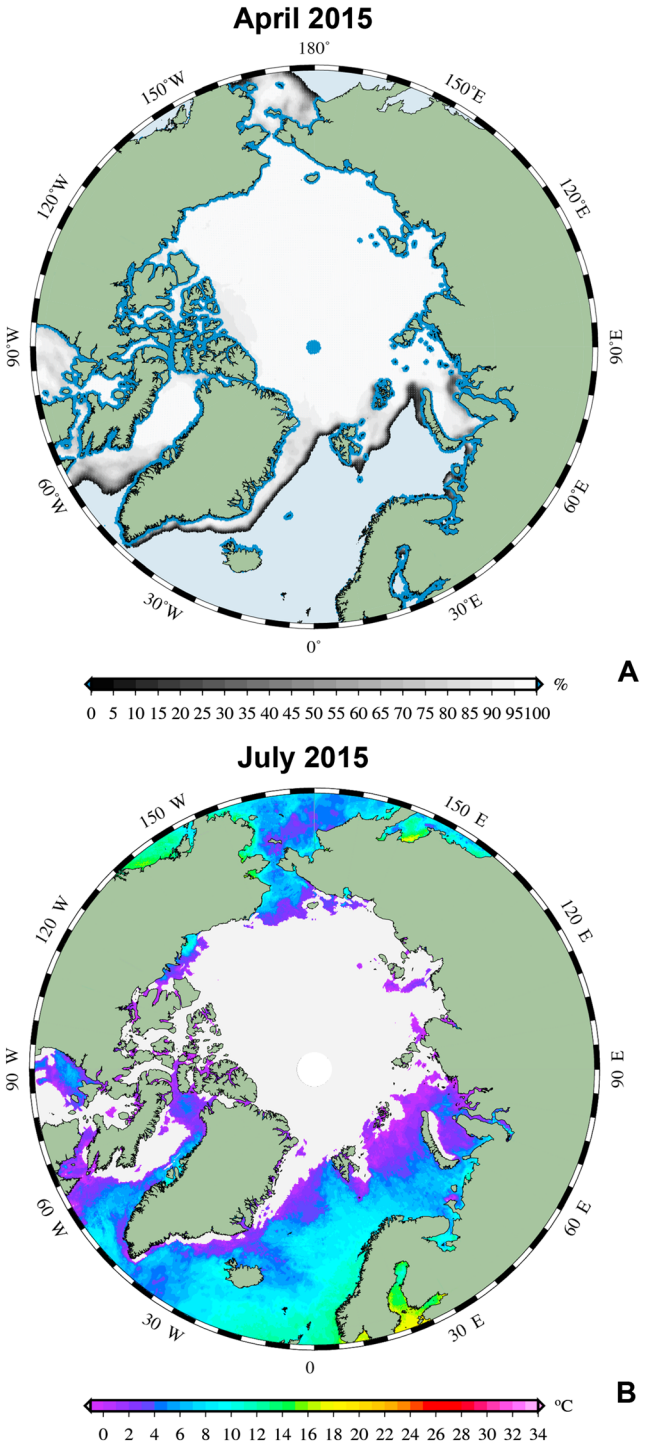

Figure 2. Examples of the modern coverage of the satellite (a) sea ice concentrations and (b) sea surface temperature reanalysis products used for the statistical model.

from 1978 to 2014 [*Eastwood et al.*, 2011; *Tonboe et al.*, 2015]. Again, the monthly averages were extracted for the grid points covering the positions of the surface sediment stations.

3.2. Surface Sediments

A total of 87 surface sediment samples (uppermost 1–2 cm) were collected along the West Greenland shelf from southern sector Qaqortoq to northern sector Uummannaq between 59°N and 72°N (Figure 1). The samples were collected during a three-leg cruise of the R/V *Paamiut* in June–July 2014. The exact locations, sampled water depths, sampling methods, lithological description, and dating information of surface sediments are given in Table 1. Sixty-six surface sediment samples were subject to analyses of natural ^{210}Pb and artificial ^{137}Cs radionuclides (emitted during the time of nuclear weapons testing) which were carried out by gamma spectrometry with a well detector (GCW4021-7500SL-RDC-6-ULB) at the Leibniz Institute for Baltic Sea Research. Thirty-two surface sediment samples with a $^{210}Pb_{unsupp.}$ activity > ~150 Bq/kg (see surface sample activity of dated multicorer data in Disko Bay [*Lloyd et al.*, 2011] and Holsteinsborg Dyb [*Sha et al.*, 2012], additional unpublished multi corer data, and by Th. J. Andresen, personal communication, 2016) which also yield traces of artificial radionuclide ^{137}Cs are regarded as "modern" and have been selected for the transfer function development (for details see Table 1; note that a few samples show ^{210}Pb values slightly lower than 150 Bq/kg but still contain traces of ^{137}Cs). In addition, three non-dated samples were also regarded as modern, based on their favorable locations and similarity in species composition with neighboring stations (Table 1). All samples valid for statistical analysis (i.e., 35 samples) span the West Greenland shelf reflecting the regional hydrographic gradients (see Figures 1 and 2).

Samples were rinsed, cleaned (hydrochloric acid and hydrogen peroxide), and mounted on slides with Naphrax® for light microscopy following the methods described in *Krawczyk et al.* [2013]. Over 300 diatom valves were counted from each sample after *Schrader* and *Gersonde* [1978]. Resting spores

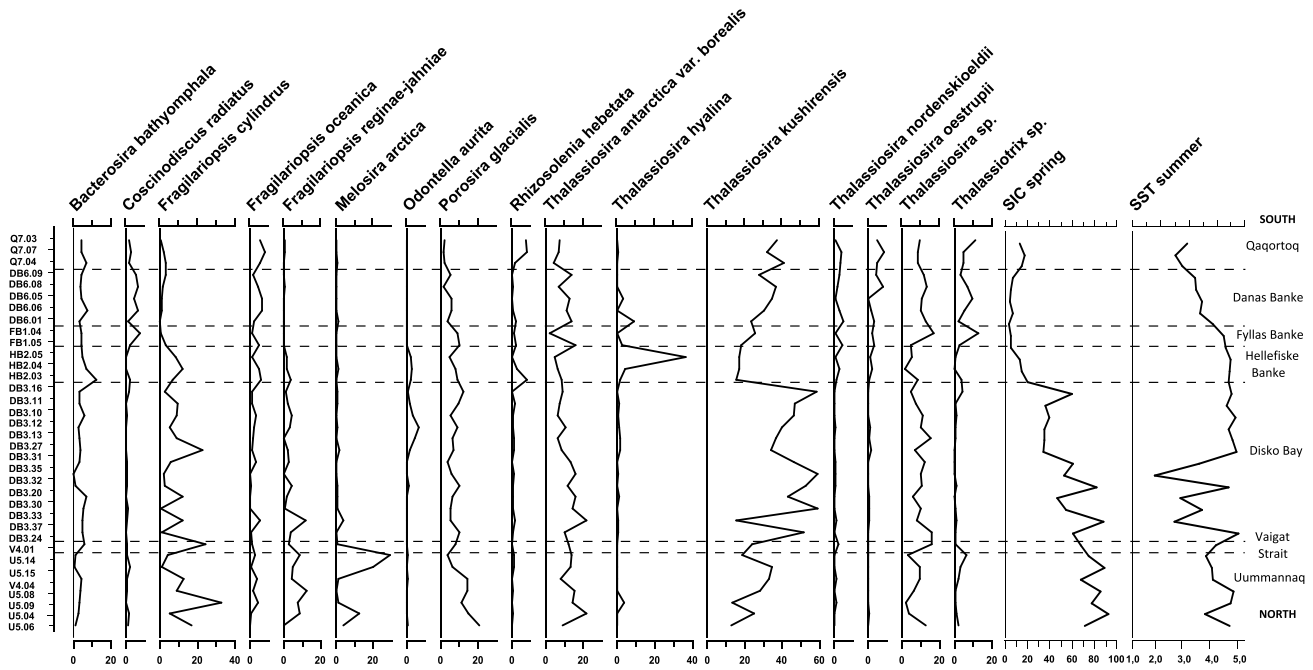

Figure 3. Distribution of dominant diatom species (>1% of diatoms in all samples) and satellite-derived environmental variables estimated for spring (SIC) and summer (SST) seasons along a transection on the West Greenland shelf. Regions are marked on the plot.

of *Chaetoceros* spp. were excluded from total counts. For the statistical analyses, the percent species abundance was used. Identification of diatom species was based on *Fryxell* [1975], *Syvertsen* [1979], *Hasle* and *Syvertsen* [1996], *Metzeltin* and *Witkowski* [1996], *Witkowski et al.* [2000], *Quillfeldt* [2001], *Throndsen et al.* [2003].

3.3. Sediment Cores

Sediment cores MSM343300 and MSM343310 were retrieved from the deep-water trough, Egedesminde Dyb, from outer SW Disko Bay (Figure 1) during a cruise of the R/V "*Maria S. Merian*" in 2007 (cruise MSM05/03) [*Harff et al.*, 2016]. The exact locations of the coring stations and sampled water depths are given in Table 1. The 1132 cm long core MSM343300 was sampled at 4–8 cm intervals, while the 939 cm long core MSM343310 was sampled at 1–2 cm intervals (for 0–10 cm) and 4 cm intervals (for 10–939 cm). A total of 424 samples were prepared for diatom analysis following the methods described in *Krawczyk et al.* [2013]. Similarly to surface sediments (see above), over 300 diatom valves were counted per sample on a *Chaetoceros*-free basis and percent species abundance was used for statistical analyses.

The chronology for both cores is based on 27 accelerator mass spectrometry (AMS) ^{14}C dates from mollusk shells and benthic foraminifera (17 dates for MSM343300 and 20 dates for MSM343310; marked on Figures 6 and 7). AMS ^{14}C dates were calibrated with the Marine09 [*Reimer et al.*, 2009] calibration curve using OxCal 4.1 [*Bronk Ramsey*, 2009] and the marine reservoir age estimated to ΔR of 140 ± 35 years [*Lloyd et al.*, 2011]. For full details of core chronologies see *Perner et al.* [2011, 2013] and *Jennings et al.* [2014]. MSM343310 has a relatively consistent sedimentation rate, averaging 2.7 mm/yr. In contrast, MSM343300 has a low sedimentation rate in the upper core section, averaging 0.64 mm/yr (0–592 cm) and a very high sedimentation rate in the lower core section, i.e., 7.8 mm/yr (592–1132 cm). MSM343300 covers the time interval ~10.9–0.84 cal ka B.P., while MSM343310 covers the time interval ~3.6–0.15 cal ka B.P. The core chronology of MSM343310 is based on a larger number of AMS ^{14}C dates. The diatom record was divided into local diatom assemblage zones (LDAZ) generated by cluster analysis (constrained incremental sums of squares) using TILIA program [*Grimm*, 1993].

3.4. Statistical Analysis

The relationships between environmental variables and *Chaetoceros*-free diatom data (%) from the surface sediments (i.e., 35 samples) were analyzed using canonical correspondence analysis (CCA). The

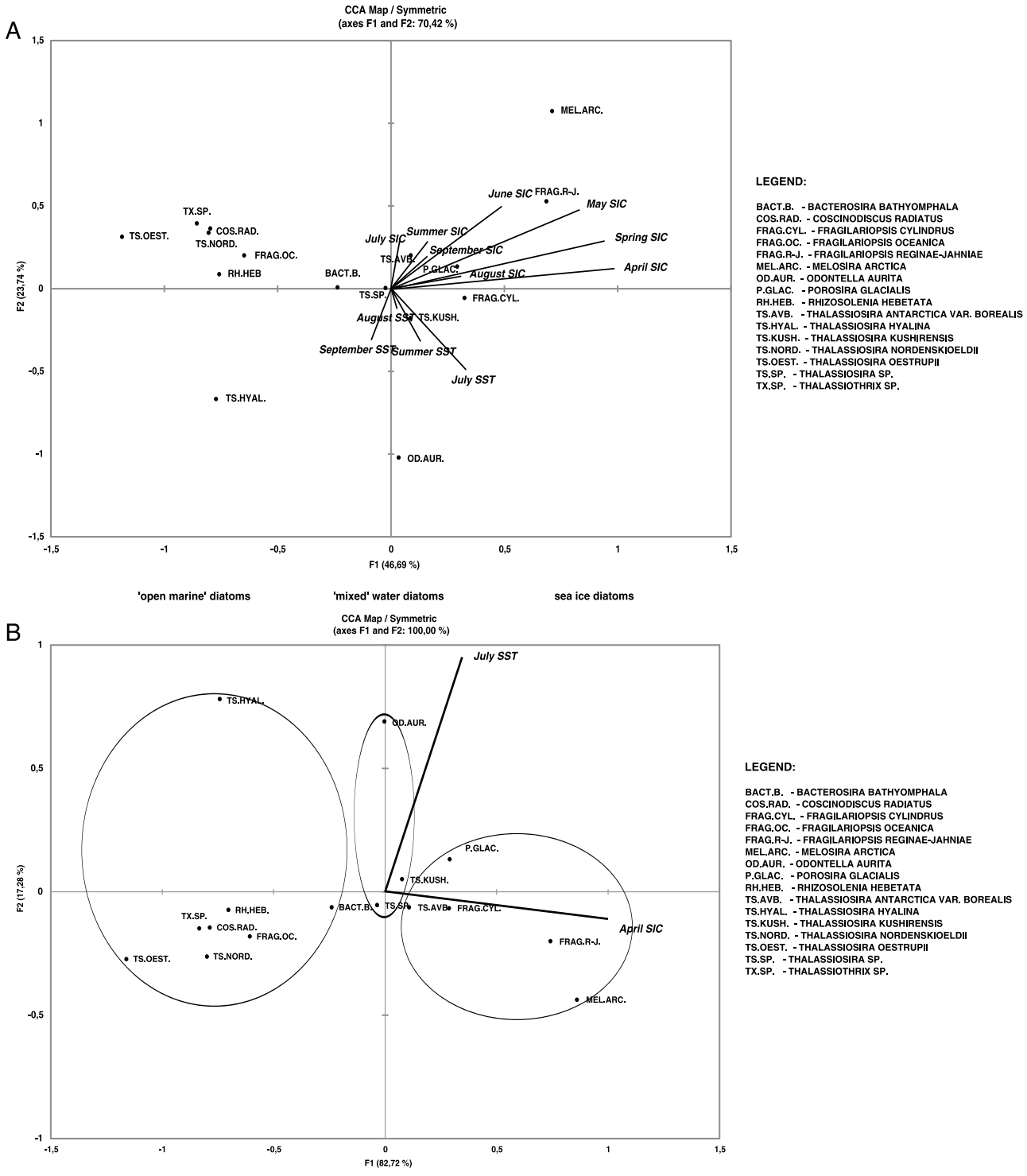

Figure 4. (a) Ordination diagram of dominant diatom species (>1% of diatoms in all samples) and all tested environmental variables (see Table 2a) along the two CCA axes. (b) Ordination diagram of dominant diatom species (>1% of diatoms in all samples) and dominant environmental variables, i.e., April SIC and July SST along the two CCA axes. Three groups of species can be identified: sea ice diatoms (to the right), "open marine" diatoms (to the left), and "mixed" water diatoms (in the middle). The highlighted groups are supported by the principal factor analysis (see Table S1). Full species names are given in the legend.

Table 2a. Results of Partial CCA to Investigate the Importance of Individual Variables[a]

Canonical Correspondence Analysis		
Variable	Percent of Variance Explained by Variable	*P* value
April SIC	**17.2**	**<0.0001**
May SIC	14.5	<0.0001
June SIC	7.1	0.06
July SIC	1.6	0.4
August SIC	3.0	0.06
September SIC	2.3	0.13
Spring SIC (Average Apr–May)	16.3	<0.0001
Summer SIC (Average Jun–Sep)	2.2	0.01
April SST	-	-
May SST	-	-
June SST	-	-
July SST	**11.0**	**<0.0001**
August SST	8.7	0.04
September SST	7.8	0.03
Summer SST (Average Jul–Sep)	3.1	0.36

[a]*P* values represent the statistical significance of the relationship between samples and variables. Best scores are shown in bold.

environmental variables are monthly averaged values of SIC (%) and SST (°C) from the last ~30 years. The environmental variables used in the CCA correspond to the months of phytoplankton (diatom) blooms identified along the West Greenland coast, i.e., from April to September. Peaks in biomass producing phytoplankton blooms (i.e., chlorophyll *a* concentrations) start already in April with highest primary production reported between May and July along the West Greenland shelf [*Boertman and Mosbech*, 2011; *Boertmann et al.*, 2013]. In the SW Greenland area, a high biomass is maintained throughout the summer until September/October [*Arendt et al.*, 2013; *Juul-Pedersen et al.*, 2015]. The winter months (November–March) were excluded from the analysis as poor light conditions in the Arctic and sub-Arctic regions during winter do not favor phytoplankton blooms [*Juul-Pedersen et al.*, 2014; *Krawczyk et al.*, 2015]. The independence and relative strength of individual monthly variables were estimated using a series of partial

Table 2b. Results of Transfer Function Methods' Tests, Where WA-PLS Is the Weighted-Averaging Partial Least Squares, ML Is the Maximum Likelihood, and (W)MAT Is the (Weighted) Modern Analogue Technique[a]

Transfer Function				
Variable	Test Method	RMSE	r^2	MaxBias
July SST	WA-PLS Component 1	0.91761	0.35956	1.5687
July SST	WA-PLS Component 2	0.75354	0.56811	1.1424
July SST	WA-PLS Component 3	0.64227	0.68624	0.77112
July SST	WA-PLS Component 4	0.54312	0.77564	0.73961
July SST	**WA-PLS Component 5**	**0.39545**	**0.88106**	**0.56571**
July SST	ML	1.2501	0.26152	2.4422
July SST	MAT	1.1357	0.10481	2.0248
July SST	wMAT	1.0768	0.18637	1.8991
April SIC	WA-PLS Component 1	10.4467	0.893464	12.1894
April SIC	WA-PLS Component 2	8.84199	0.923681	10.9486
April SIC	WA-PLS Component 3	6.42372	0.959718	5.04095
April SIC	WA-PLS Component 4	5.11854	0.974424	3.29237
April SIC	WA-PLS Component 5	4.32102	0.981773	5.80612
April SIC	**ML**	**5.732**	**0.97**	**6.8677**
April SIC	MAT	16.814	0.83135	24.312
April SIC	wMAT	14.792	0.85826	22.39

[a]RMSE, coefficient of determination between observed and estimated variable (r^2), and maximum bias (MaxBias) are given for tested variables. Best scores are shown in bold.

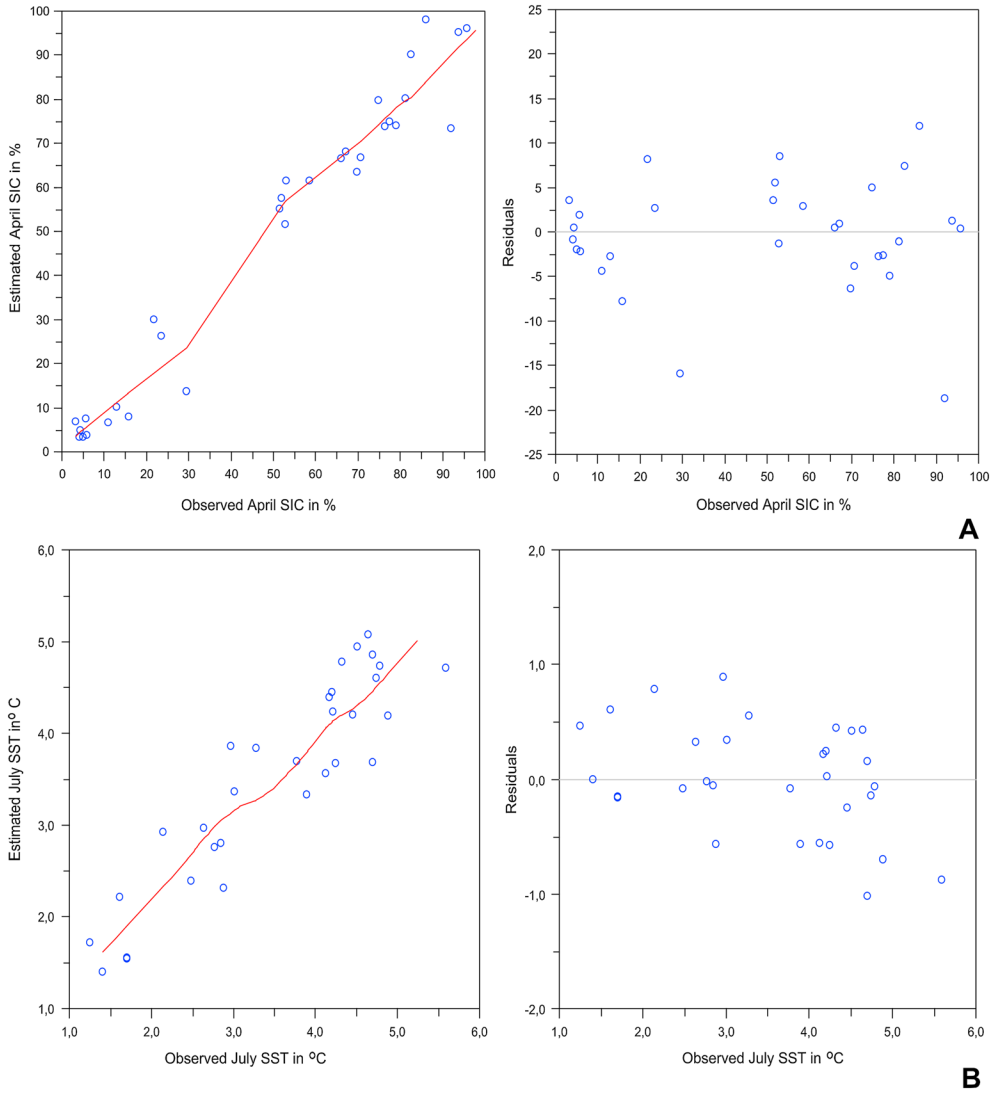

Figure 5. Regression plots between the (left) observed and estimated and (right) observed and residual values of April SIC (a) using maximum likelihood method and July SST (b) using weighted-averaging partial least squares. The r^2 for April SIC is 0.97 and r^2 for July SST is 0.88.

CCAs [*Borcard et al.*, 1992]. Permutation test (1000 permutations) was carried out to estimate the statistical significance (*P* values) of relationships between environmental variables and diatom species. CCA was carried out using the xlstat program.

Surface sediment data were used to convert downcore diatom counts to quantitative SIC and SST using weighted-averaging partial least squares (WA-PLS) [*ter Braak and Juggins*, 1993], maximum likelihood (ML), and modern analogue technique (MAT) [*Upton and Cook*, 2002] transfer function methods. The WA-PLS method estimates species' optimal abundance in response to a tested environmental variable [e.g., *Miettinen et al.*, 2011]. The ML method estimates the expected/reconstructed environmental variable that would give the maximum probability of the observed diatom assemblages, whereas the MAT evaluates the best species assemblages' match between the fossil sample and the nearest available surface sediment sample assuming that the same diatom assemblage reflects the same environmental conditions [*Upton and Cook*, 2002]. Detailed descriptions of each diatom transfer function method can be found in previous studies [e.g., *Justwan and Koç*, 2008; *Miettinen et al.*, 2011]. Transfer functions were carried out using C2 program [*Juggins*, 2007].

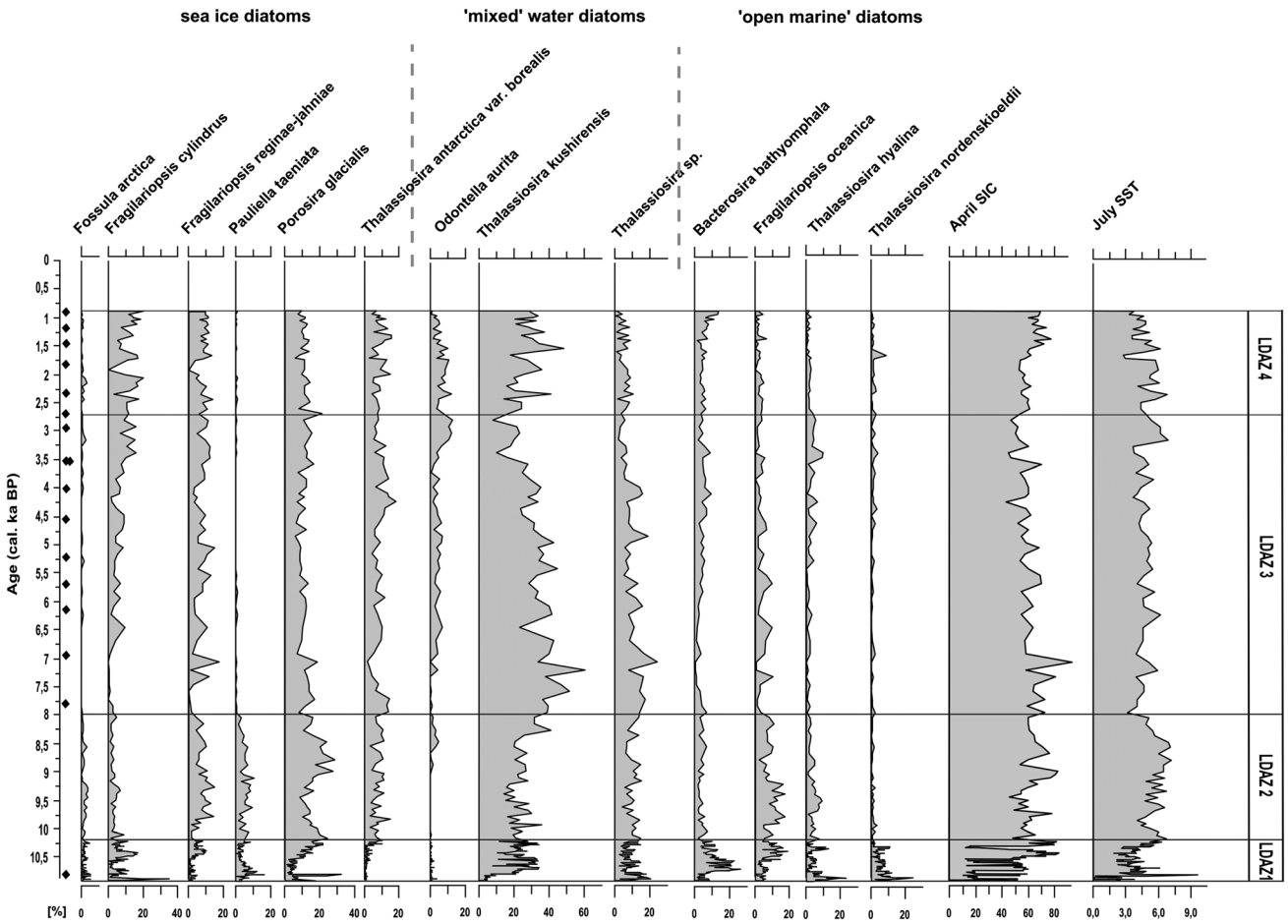

Figure 6. The dominant diatom species (>1% of diatoms in all samples) along with reconstructed April SIC and July SST from MSM343300, Disko Bay, plotted against age (cal ka B.P.). The location of the 17 AMS ^{14}C dates is marked next to the "age" axis (black diamonds). Dominant diatom species were grouped into three key assemblages according to their ecological preferences.

4. Results

4.1. Modern Diatom Distribution

The modern distribution of diatom species along the West Greenland coast (Figure 3) is closely linked to modern oceanographic conditions as identified by satellite-derived sea ice concentration (SIC) and sea surface temperature (SST). The southernmost stations, including Qaqortoq and Danas Banke sectors, are characterized by *Thalassiosira kushirensis*, *Thalassiosira* sp., *Thalassiosira oestrupii*, *Fragilariopsis oceanica*, *Thalassiothrix* sp., *Coscinodiscus radiatus*, *Thalassiosira nordenskioeldii* and *Rhizosolenia hebetata*. *Thalassiosira hyalina*, *Bacterosira bathyomphala*, *F. oceanica*, *R. hebetata*, *Odontella aurita*, and *T. nordenskioeldii* are common from Fyllas Banke and Hellefiske Banke sectors. Disko Bay stations are dominated by *T. kushirensis* and *Thalassiosira* sp., together with higher abundances of *Thalassiosira antarctica* var. *borealis*, *Fragilariopsis cylindrus*, and *O. aurita*. The northernmost stations including Vaigat Strait and Uummannaq region are characterized by *F. cylindrus*, *Fragilariopsis reginae-jahniae*, *Porosira glacialis*, *T. antarctica* var. *borealis*, and *Melosira arctica*. The modern SIC estimated for the spring season (i.e., April–May) [cf. *Krawczyk et al.*, 2015] shows highest values north of Fyllas Banke (Figure 3). Maximum SIC (>60%) is recorded in Vaigat and Uummannaq sectors. The SIC in the southern sectors (i.e., south of Fyllas Banke) remains low (average of 7.9%). These southern sectors display rather low SST during the summer period (July–September, when data points are available for all sampling stations; see below) with an average of 3.1°C. However, the maximum SST values (>4.4°C) are recorded in Hellefiske Banke and in Disko Bay (Figure 3), offshore from the glacier front. Moderate SSTs are recorded from Vaigat Strait and Uummannaq area (average of 4°C).

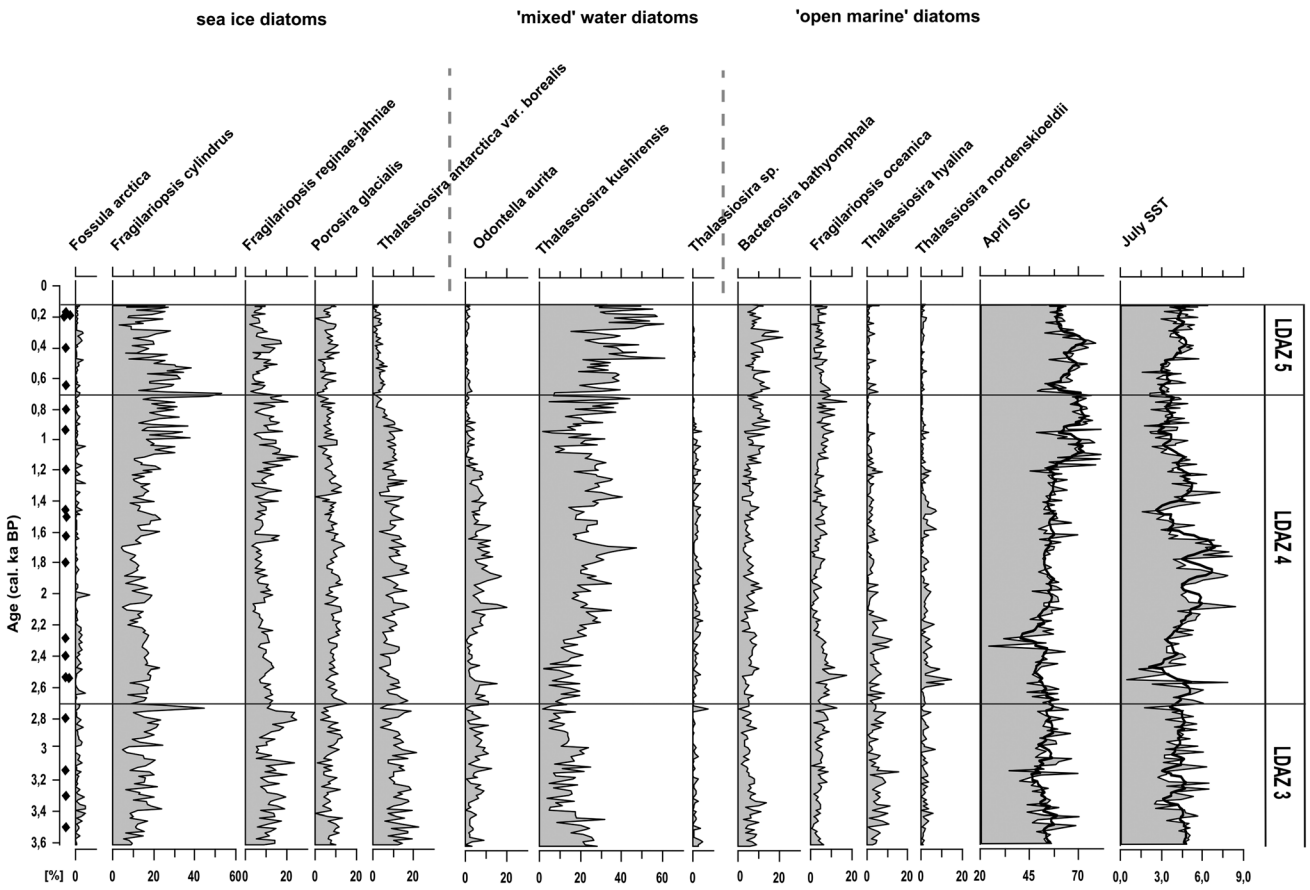

Figure 7. The dominant diatom species (>1% of diatoms in all samples) along with reconstructed April SIC and July SST (black curves representing 5-point running mean) from MSM343310, Disko Bay, plotted against age (cal ka B.P.). The location of the 20 AMS ^{14}C dates is marked next to the "age" axis (black diamonds). Dominant diatom species were grouped into three key assemblages according to their ecological preferences.

4.2. Species-Environment Relationship

The ordination diagrams of the diatom data and environmental variables (SIC and SST along the CCA Axes 1 and 2) are shown in Figure 4. Diatom data include 16 dominant diatom species, i.e., >1% of diatoms in all samples to reduce the impact of rare taxa, benthic cosmopolitan, and undetermined species. Both SIC and SST were tested separately for each month corresponding to diatom bloom season, i.e., from April to September and for average of spring and summer seasons (Figure 4a and Table 2a). For SST we included only months when no persisting sea ice cover was recorded (no missing SST data points), i.e., July–September. This is also supported by a low % of variation in data explained by SIC (less than 4%; see Table 2a). Previous studies in the area have also shown the presence of diatom species associated with sea ice at stations near the sea ice margin in June [*Jensen*, 2003; *Krawczyk et al.*, 2014], which may bias the analyses for SST.

The partial CCAs show that April SIC, May SIC, and July SST explain the most variance in the diatom data from surface sediments compared to other tested months, 17.2%, 14.5%, and 11%, respectively (see Table 2a). Given that maximum sea ice extent along the coast is observed in March/April, peaks in diatom blooms (i.e., phytoplankton blooms) occur in April (as noted in section 4.3), we use April SIC as the indicator variable in the further statistical analysis, rather than May SIC. The correlation of variables with Axes 1 and 2 indicates that April SIC is positively correlated with Axis 1 and July SST is positively correlated with Axis 2 (Figure 4b). The diatom species can be divided into three assemblages based on their modern ecology and a combination of visual inspection of species' position in relation to the tested variables on the CCA diagrams (Figure 4) and quantitative establishment of indicator species using principal factor analysis (Table S1 in the supporting information). Detailed descriptions of modern ecological preferences (with literature sources) of most of the identified dominant diatoms can be found in *Krawczyk et al*. [2013, 2014]. The identified three assemblages

are (1) sea ice diatoms correlated with high April SIC, (2) "open marine" diatoms correlated with low April SIC (i.e., open water conditions), and (3) "mixed" water diatoms influenced by both April SIC and July SST (Figure 4 b). Sea ice diatoms plotting to the right of the CCA Axis 1 are represented by *F. cylindrus*, *F. reginae-jahniae*, *M. arctica*, *P. glacialis*, and *T. antarctica* var. *borealis*. "Open marine" diatoms plotting to the left of the CCA Axis 1 are represented by *F. oceanica*, *B. bathyomphala*, *T. nordenskioeldii*, *T. hyalina*, *Thalassiothrix* sp., *T. oestrupii*, *R. hebetata*, and *C. radiatus*. "Mixed" water diatoms plotting in the middle of the biplot are represented by *O. aurita*, *Thalassiosira* sp., and *T. kushirensis*. In previous, qualitative diatom-based study from Disko Bay using sediment core MSM343310 [*Krawczyk et al.*, 2013] the aforementioned species belonging to the genus *Fragilariopsis* were classified as (sea) ice associated diatoms while the species belonging to genus *Thalassiosira* as northern cold-water diatoms. This shows a close similarity to the present quantitative study. The exception to this is *T. kushirensis* which was classified as a warm/temperate water species [*Krawczyk et al.*, 2013]. More recently, *T. kushirensis* has been described both as an Arctic species [*Weckström et al.* 2014] and as a species associated with slightly warmer summer waters [*Krawczyk et al.*, 2014; *Moros et al.*, 2016].

4.3. Transfer Function

The weighted averages-partial least squares (WA-PLS), maximum likelihood (ML), and modern analogue technique (MAT) diatom transfer functions were tested for April SIC and July SST (Table 2b). It should be mentioned that although April SIC and July SST explain the most variance in the diatom data, the actual values are rather small (17.2% and 11%, respectively). A reliable transfer function should have high values of coefficient of determination between observed and estimated variable (r^2) and low values of RMSE and maximum bias [*Birks*, 1995, 1998]. According to model performance for April SIC, both WA-PLS and ML show very good scores with high values of r^2 and low values of RMSE and maximum bias (see Table 2a). However, in reconstructed April SIC the WA-PLS method using four and five components (with highest values of r^2) displays values outside the range of 0–100%, whereas ML displays values within this range; hence, we use the ML method as the most reliable transfer function for reconstructing April SIC. The MAT method, on the other hand, shows too high values of RMSE and maximum bias. For July SST, the WA-PLS using five components shows the best scores with highest values of r^2 (0.88) and lowest values of RMSE ($\pm$0.39°C) and maximum bias (0.56°C). The ML and MAT methods both show very low r^2; hence, WA-PLS with five components shows a better correlation between observed and estimated July SST.

The strong correlation between the observed and estimated April SIC using ML method (Figure 5a) and July SST using WA-PLS method (Figure 5b) indicates that the generated diatom transfer functions are reliable. It should be noted that the range of SSTs observed in summer (i.e. ~1–6°C) in the reference diatom data set is rather small. Also, the reconstructed July SST occasionally shows values above this range (see Figures 6 and 7) but mostly within the estimated error. Thus, in the following interpretation of the reconstructed oceanographic conditions we primarily focus on quantitative estimates of April SIC which is supplemented by identified trends and averaged values of July SST.

4.4. Stratigraphy of the Cores

A total of 207 diatom taxa were identified from the sediment cores MSM343300 and MSM343310. Of these taxa 178 were determined to species and 29 to generic levels. The most abundant species in these sediment cores are *T. kushirensis*, *F. cylindrus*, *P. glacialis*, *T. antarctica* var. *borealis*, and *F. reginae-jahniae.* All dominant species (>1% of diatoms in all samples) along with reconstructed April SIC and July SST are plotted in Figures 6 and 7. The dominant species are grouped into three assemblages based on the understanding of their ecological preferences and modern distribution [*Krawczyk et al.*, 2013, 2014]. The following section provides description of changes in April SIC and July SST based on diatom record during six distinguished time intervals, i.e., local diatom assemblage zones (LDAZs).

4.4.1. LDAZ1: Time Interval ~10.9–10.2 cal ka B.P.

LDAZ 1 is characterized by the greatest recorded variability in April SIC composed of six distinct peaks (Figure 6). These peaks are represented mainly by sea ice diatoms, such as *F. cylindrus*, *Pauliella taeniata*, and *P. glacialis*. In this time interval April SIC recorded the lowest average value of 44% throughout the study with absolute minima of 8.8% and 10.3% at 10.85 cal ka B.P. and 10.8 cal ka B.P., respectively (Figure 6). Nevertheless, the overall trend in April SIC shows an increase. July SST showed the lowest recorded values with an average of 3.4°C, but with a strongly increasing trend (Figure 6). This trend is reflected by the "mixed" water diatom *T. kushirensis* and an "open marine" species *F. oceanica* (Figure 6).

4.4.2. LDAZ 2: Time Interval ~10.2–8.0 cal ka B.P.

This zone is characterized by a high average April SIC (63%) with a rather stable trend (Figure 6). The sea ice diatoms contributing most to this high value are *F. reginae-jahniae*, *P. taeniata*, *P. glacialis* and *T. antarctica* var. *borealis*. *P. taeniata* and *P. glacialis* reached the highest abundances in this time interval (average of 4% and 16%, respectively) throughout the study. Interestingly, *P. taeniata* is virtually absent after 8.0 cal ka B.P. (Figure 6). July SST reaches the maximum average value throughout the study of 5.6°C in this zone (Figure 6). This pattern was represented by increase in abundance of all "mixed" water diatoms in this zone, i.e., *T. kushirensis*, *Thalassiosira* sp., and *O. aurita* together with an "open marine" diatom *F.* oceanica (Figure 6).

4.4.3. LDAZ 3: Time Interval ~8.0–2.7 cal ka B.P.

LDAZ 3 is marked by a slight decrease in April SIC with an average of 58% (Figure 6). The lowest value of 42% was recorded at 4.2 cal ka B.P. This is reflected by a decrease in abundance of sea ice diatoms (i.e., *P. taeniata* and *P. glacialis*) and an increase in abundance of "open marine" diatoms, i.e., *B. bathyomphala*, *T. hyalina*, and *T. nordenskioeldii* (Figure 6). July SST recorded lower average value of 4.7°C, compared to the previous zone (Figure 6). July SST showed a rather stable trend in this time interval with a slight increase toward the end. This increase is reflected by increase in abundance of a "mixed" water diatom *O. aurita* (Figure 6). The MSM343310 record generally showed a rather stable trend in April SIC and July SST after ~3.6 cal ka B.P. (Figure 7).

4.4.4. LDAZ 4: Time Interval ~2.7–0.7 cal ka B.P.

The description of diatom record for LDAZ 4 and the following LDAZ 5 is based on MSM343310 (Figure 7) as this sediment core better reflects the late Holocene oceanographic conditions (see section 3). Nevertheless, both MSM343300 and MSM343310 show an overall increase in April SIC (Figures 6 and 7). Highest values of April SIC were recorded from 1.2 to 0.7 cal ka B.P. with an average of 70% (Figure 7). These highest values are driven by a strong increase in abundance of *F. cylindrus* and also *F. reginae-jahniae*. July SST records a slightly lower average value of 4.3°C compared to the previous zone (Figure 7). Highest July SSTs were recorded between 2.3 and 1.6 cal ka B.P. (average of 5.3°C) driven by high abundances of "mixed" water diatoms in this zone, i.e., *T. kushirensis* and *O. aurita* (Figure 7). This high July SST was followed by a sharp decrease, particularly pronounced after 1.0 cal ka B.P. (average of 3.4°C).

4.4.5. LDAZ 5: Time Interval ~0.7–0.15 cal ka B.P.

April SIC showed a generally decreasing trend during this time interval, yet with a relatively high average of 64% (Figure 7). This decreasing trend is clearly influenced by a significant decrease in abundance of the sea ice diatom *F. cylindrus* (Figure 7). Nevertheless, two pronounced peaks, mirroring peaks in abundance of the sea ice diatom *F. reginae-jahniae*, were recorded at ~0.53 cal ka B.P. (76%) and ~0.4 cal ka B.P. (81%). In contrast, July SST showed a pronounced increase in this zone with an average value of 4°C (Figure 7). This increase is reflected by a strong increase in abundance of the "mixed" water diatom *T. kushirensis*. The highest July SST was recorded after 0.4 cal ka B.P. (Figure 7).

5. Discussion

5.1. Regional Diatom Data Set

The modern distribution of diatom species along the West Greenland coast shows a clear latitudinal grouping. Statistical analysis shows that this latitudinal pattern is largely influenced by the distribution of spring sea ice cover (i.e., April sea ice concentration; SIC) and summer water temperature (i.e., July sea surface temperature; SST) (Figures 3 and 4). Based on modern ecology of diatoms and a combination of CCA (Figure 4) and principal factor analysis (Table S1), we distinguish three groups: (1) sea ice diatoms influenced by northern sea ice cover, (2) "open marine" diatoms influenced by southern ice-free waters, and (3) "mixed" water diatoms influenced by sea ice cover and warmer summer waters. Nevertheless, April SIC and July SST do not explain most of the variance in the diatom data set suggesting that other, probably nonphysical drivers, such as nutrient supply or succession patterns among microplankton species (compare with *Krawczyk et al.* [2015]) might play an important role in diatom distribution along the West Greenland coast. The transfer function developed here relies on satellite-derived environmental variables, hence, it is limited how much of the actual variance in diatom assemblages, including biological aspects of the marine ecosystems, can be explained. However, a strong correlation between studied modern diatom species and environmental variables and low estimated error values (Tables 2a and 2b) make this modern data set useful and reliable in quantitative reconstructions using the transfer function technique.

5.2. Transfer Function Reconstruction

Our quantitative reconstruction of oceanographic conditions in Disko Bay reflects significant changes in April SIC supplemented by changes in July SST offshore West Greenland during the last ~11,000 years. In this study we compare our quantitative diatom-based reconstructions from Disko Bay with corresponding studies with quantitative data from the western sector of the North Atlantic Ocean throughout the Holocene (Figure 8). These reconstructions are discussed in relation to the climatic trends from the Greenland-Arctic region (Figure 8). This quantitative study supports the general findings regarding surface water conditions described from previous diatom-based qualitative reconstructions from Disko Bay using the same sediment cores covering the middle to late Holocene period [*Krawczyk et al.*, 2013; *Moros et al.*, 2016]. In particular, in aforementioned qualitative reconstructions relative abundances of diatom species regarded as "(sea) ice associated" are convergent with our April SIC reconstruction for the last ~8 cal ka B.P.; relative abundances of "warmer water" diatoms are in line with our July SST record mostly for the late Holocene. For detailed interpretations of local surface and subsurface water conditions in Disko Bay using multiple proxies from the same sediment cores, i.e. diatoms, alkenones, dinocysts, and benthic foraminifera, please see *Moros et al*. [2016].

5.2.1. Early Holocene (~10.9–8.0 cal ka B.P.)

Stage I (LDAZ 1). Several strong peaks in April SIC with amplitude of over 40% were recorded between ~10.9–10.2 cal ka B.P. suggesting centennial-scale pulses of strong spring time melting of sea ice (Figures 8c and 9). Very high sedimentation rate and high content of glacial detritus recorded in the sediment core (i.e., MSM343300) only in this time interval [*Harff et al.*, 2016] suggest a strong freshwater input associated with glacial discharge of the western Greenland Ice Sheet. The identified oceanographic conditions correspond to a strong warming trend in atmospheric temperature over the Greenland-Arctic region (Figures 8a and 8b) [*Alley et al.*, 1999; *Vinther et al.*, 2009] and significant, continued deglaciation of the western Greenland Ice Sheet. The deglaciation of the central Disko Bay is dated for 10.2 cal ka B.P. based on the westward retreat of Jakobshavn Isbrae [*Lloyd et al.*, 2005]. Enhanced ice sheet ablation in Disko Bay was reported between 10.9 and 9.5 cal ka B.P. [*Jennings et al.*, 2014]. In the northern Baffin Bay region calving margins of the Laurentide Ice Sheet were suggested to produce large meltwater pulses along the central West Greenland margin by ~10.5 cal ka B.P. [*Jennings et al.*, 2014; *Sheldon et al.*, 2016]. *Roberts et al.* [2009] indicate retreat of Greenlandic glaciers from the continental shelf until ~10.0 cal ka B.P. A strong decrease in May SIC from over 50% to ~10% was recorded from the north Iceland shelf in this period (Figure 8e) [*Justwan and Koç*, 2008] suggesting a retreat of sea ice cover in the North Atlantic region. This decrease is accompanied by a strong increase in August SST (Figure 8f) [*Justwan and Koç*, 2008] in the area. Also in Reykjanes Ridge, south of Iceland, summer SSTs were relatively high from 11.0 to 10.0 ka B.P. (Figure 8h) [*Andersen et al.*, 2004b]. Stronger influence of warmer waters along with minimal sea ice cover was suggested between 11.3 and 9.9 cal ka B.P. off the south coast of Newfoundland [*Pearce et al.*, 2014]. These reconstructions of summer warming in surface waters alongside increase in July SST recorded from this study can be ascribed to high summer insolation identified at the beginning of the Holocene [*Andersen et al.*, 2004b].

Stage II (LDAZ 2). High April SIC accompanied by high July SST recorded between ~10.2 and 8.0 cal ka B.P. (Figures 8c and 8d and 9) indicate a strong signal of spring time melting throughout the Holocene. This can also indicate a long bloom period producing high abundances of spring and summer species. Interestingly, *Pauliella taeniata* shows highest abundances in the early Holocene but very little presence after ~8.0 cal ka B.P. (Figure 6). This species is known as a brackish-water form, common mainly in Arctic areas influenced by freshwater input from Canadian and Siberian rivers and also abundant in the Baltic Sea low-salinity waters [*Hasle and Syvertsen*, 1996]. The peak in abundance of this species would support the interpretation of a strong freshwater discharge from the Greenland Ice Sheet, as well as from the Canadian Arctic, persisting into the early Holocene [*Williams et al.*, 1995]. This interpretation of continued strong melting with warmer summer waters in Disko Bay corresponds to the significant climate warming in the early Holocene (Figure 8a and 8b) [*Alley et al.*, 1999; *Vinther et al.*, 2009], widely recognized in the Northern Hemisphere [e.g., *Kullman*, 1999; *Kaufman et al.*, 2003]. Oceanic and climatic warming seems to coincide with maximum thinning of the Greenland Ice Sheet in this period [*Vinther et al.*, 2009]. In outer Disko Bay, strong meltwater influence associated with final deglaciation of the inner continental shelf and retreat of the Greenland Ice Sheet into the fjords and on land prevailed until ~8.0–7.5 cal ka B.P. [*Jennings et al.*, 2014; *Moros et al.*, 2016]. In addition, the retreat of Jakobshavn Isbrae into the fjord system (Jakobshavn Isfjord) close to the approximate twentieth century margin was most likely associated with enhanced inflow of the West Greenland Current

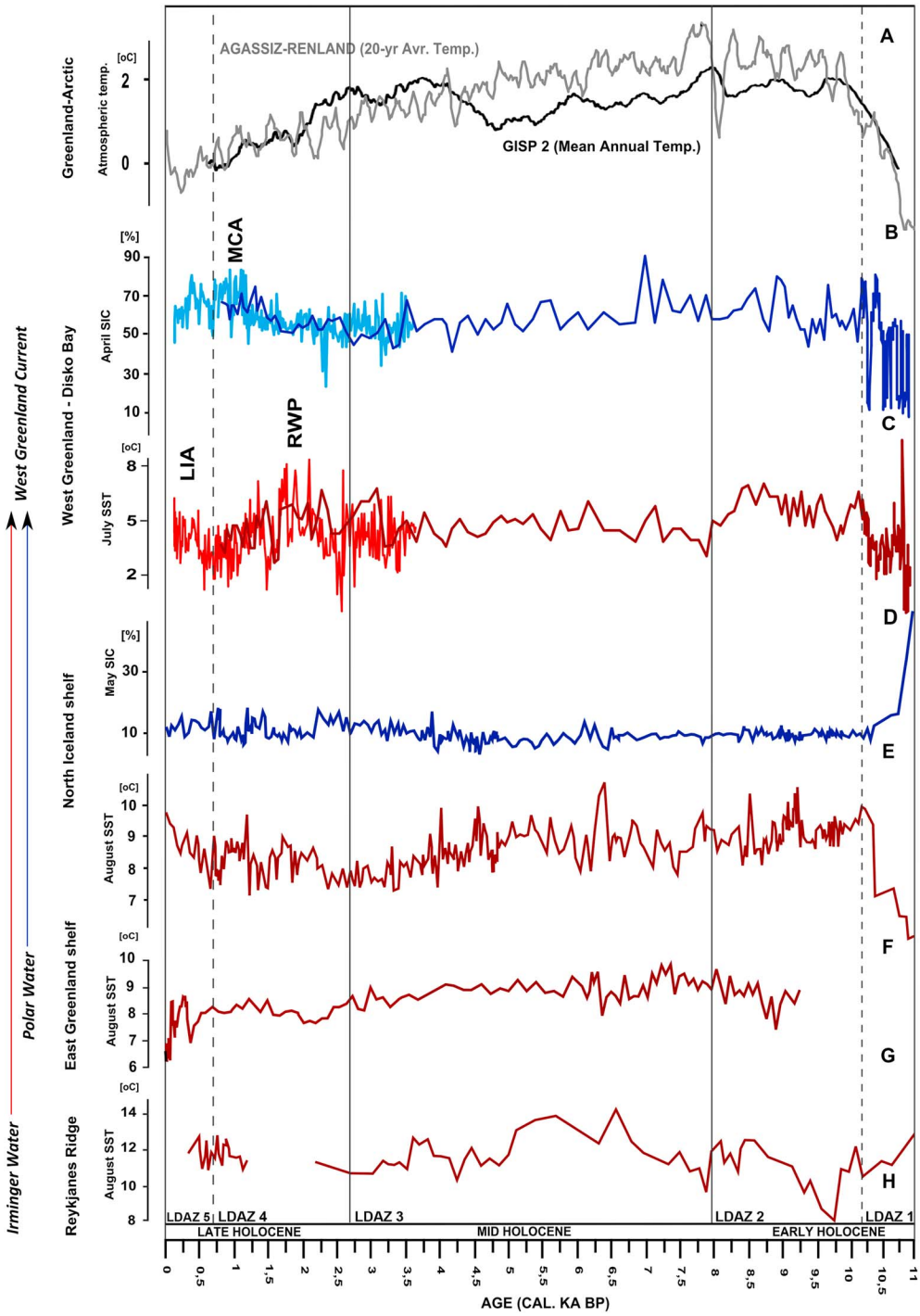

Figure 8. Comparative data sets from the Arctic and North Atlantic region presented from northern (top) to southernmost (bottom) with information on the distribution of the key water masses. (a) mean annual temperature reconstructed from the GISP2 ice core [*Alley et al.*, 1999], (b) The 20 year average temperature (5-point mean) reconstructed from averaged ice core data from Agassiz-Renland [*Vinther et al.*, 2009], (c) reconstructed April SIC from diatom record from MSM343300 (dark blue curve) and MSM343310 (light blue curve) (this study), (d) reconstructed July SST from diatom record from MSM343300 (dark red curve) and MSM343310 (light red curve) (this study), (e) reconstructed May SIC and (f) August SST from diatom record from core MD99-2269, North Iceland shelf [*Justwan and Koç*, 2008], (g) diatom-based reconstruction of the August SST from core CR 19/5, East Greenland shelf [*Andersen et al.*, 2004a], and (h) diatom-based reconstruction of the August SST from core LO09-14, Reykjanes Ridge [*Andersen et al.*, 2004b]. The time intervals: the Roman Warm Period (RWP), the Medieval Climate Anomaly (MCA), and the Little Ice Age (LIA) based on the NW European system are included (see in text). Local diatom assemblage zones (LDAZ) are marked on the plot.

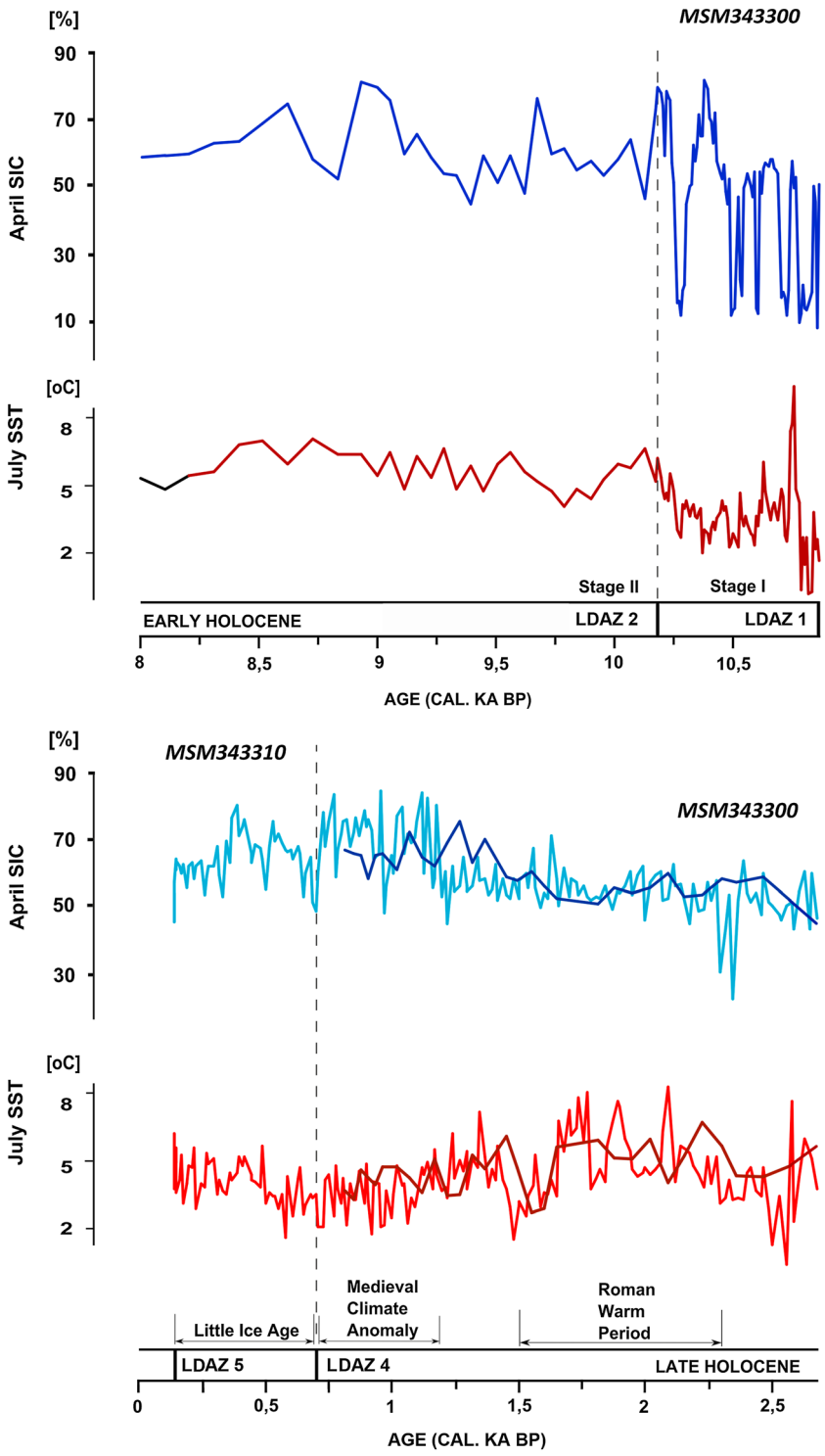

Figure 9. Reconstructed April SIC and July SST from MSM343300 (dark blue/red curves) and MSM343310 (light blue/red curves), Disko Bay, for early and late Holocene. Local diatom assemblage zones (LDAZ) are marked on the plot.

(WGC) after ~9.2 cal ka B.P. [*Lloyd et al.*, 2005]. Our record of maximum July SST seems to confirm the warming within the WGC during the early Holocene, most likely derived from the warm Irminger Water. In the North Atlantic region, the early Holocene climatic warming has been attributed to an enhanced regime of the North Atlantic Current system [*Andersen et al.*, 2004a, 2004b]. A reconstructed August SST from the

Reykjanes Ridge indicates intensified Atlantic water flow after ~9.5 B.P. (Figure 8h) [*Andersen et al.*, 2004b]. Stronger influence of Atlantic water masses was recorded in the Norwegian Sea at this time [*Koç Karpuz and Jansen*, 1992; *Andersen et al.*, 2004a]. An eastward shift in the Arctic front system toward the Norwegian Sea was identified from the early to middle Holocene associated with warming in surface waters [*Moros et al.*, 2004].

5.2.2. Holocene Thermal Optimum (~8.0–2.7 cal ka B.P., LDAZ 3)

A decrease in April SIC along with July SST (Figures 8c and 8d) offshore West Greenland during this interval suggests reduced sea ice cover and melting of sea ice. Oceanographic conditions might reflect more stable spring-summer water conditions, compared to the early Holocene. These conditions correspond to relatively warm climatic conditions over Greenland and the wider Arctic region (Figures 8a and 8b) [*Alley et al.*, 1999; *Vinther et al.*, 2009], recognized as the Holocene Thermal Optimum (HTO) in the Northern Hemisphere [e.g., *Johnsen et al.*, 2001; *Jennings et al.*, 2014]. Previous studies from Disko Bay indicate a minimum Greenland Ice Sheet extent during the HTO and ocean cooling toward the end of this period (in *Moros et al.* [2016]). Other studies from West Greenland suggest a slightly later Greenland Ice Sheet minimum between 5 and 3 ka B.P. [*Ren et al.*, 2009; *Young and Briner*, 2015]. Generally low SIC between 5 and 3.8 cal ka B.P. was recorded from Vaigat Strait using recent diatom transfer function suggesting relatively warm surface water conditions with strong influence of the Irminger Current [*Sha et al.*, 2014]. On the North Iceland shelf and East Greenland shelf, generally decreasing trends in August SST were recorded throughout this period (Figures 8f and 8g) [*Justwan and Koç*, 2008; *Andersen et al.*, 2004a]. In addition, glacier advances have been reconstructed in North Iceland [*Stötter et al.*, 1999] and an increase in ice rafting offshore East Greenland for this period [*Jennings et al.*, 2002; *Moros et al.*, 2004]. This increase in iceberg rafting and glacial advance in Iceland may be linked to reduced solar irradiance [*Bond et al.*, 2001]. In contrast, a pronounced increase in August SST was recorded at the Reykjanes Ridge until ~5.0 ka B.P. (Figure 8h) [*Andersen et al.*, 2004b] associated with enhanced North Atlantic Current flow via the Irminger Current. Quantitative diatom analyses from the Norwegian Sea show warming in surface waters between 3.5 and 2.7 cal ka B.P. [*Birks and Koç*, 2002; *Berner et al.*, 2011]. The terrestrial data from Scandinavia suggest relatively mild climatic conditions at ~3.7 cal ka B.P. [*Snowball et al.*, 1999; *Hammarlund et al.*, 2002]. However, general storminess and cyclone activity identified in the North Atlantic during this period [*Andersen et al.*, 2004b; *Witak et al.*, 2005] suggest fluctuations in the North Atlantic Oscillation (NAO), as identified previously by *Giraudeau et al.* [2000] and *Andersen et al*. [2004a]. Termination of the HTO coincides with the commonly reported "Neoglacial" cooling after ~4.0–3.5 cal ka B.P. [e.g., *Andersen et al.*, 2004a; *Jennings et al.*, 2014; *Moros et al.*, 2016].

5.2.3. Late Holocene (2.7–0.15 cal ka B.P., LDAZ 4)

A rather low April SIC corresponds to the European Roman Warm Period (RWP, 2.3–1.5 cal ka B.P.) [*Seidenkrantz et al*., 2008] and a strong decrease in April SIC to the Little Ice Age, accompanied by reversed July SST trends (LIA, ~0.7–0.15 cal ka B.P.) (Figures 8c and 8d and 9) suggesting warmer surface waters. In contrast, a pronounced increase in April SIC corresponds to the European Medieval Climate Anomaly (MCA, 1.2–0.7 cal ka B.P.) [*Mann et al.*, 2009] (Figures 8c and 9). This period is also characterized by slightly cooler July SSTs indicating strong spring time melting (i.e., surface water cooling). These late Holocene trends in surface water conditions in Disko Bay were also recorded in previous studies, e.g., qualitative diatom records [*Krawczyk et al.*, 2013; *Moros et al.*, 2016], quantitative diatom sea ice record for the RWP [*Sha et al.*, 2014], dinoflagellate records for the RWP and the MCA [*Seidenkrantz et al*., 2008; *Ribeiro et al.*, 2012], and alkenone records (i.e., SST and salinity) for the MCA and the LIA (data from the same sediment cores) [see *Moros et al*., 2016, Figure 4]. In previous diatom-based studies *Krawczyk et al*. [2010, 2013] suggested that the trends identified during the MCA and LIA were linked to stronger seasonal oceanographic variability, i.e., increased spring time melting leading to cooler summer waters (MCA) and reduced spring time melting leading to warmer summer waters (LIA).

The European warm climate events of the RWP and the MCA were not recorded from reconstructed atmospheric temperatures from the Greenland-Arctic region (Figures 8a and 8b) [*Vinther et al.*, 2009]. In the North Atlantic region, the RWP was characterized by higher August SST on the North Iceland shelf (Figure 8f) [*Justwan and Koç*, 2008] and warmer conditions on the East Greenland shelf [*Jennings et al.* 2002] and Reykjanes Ridge [*Moros et al.*, 2012]. On the other hand, cooling of surface waters during the MCA was recorded across SW Greenland [*Roncaglia and Kuijpers*, 2004], Labrador Sea [*Seidenkrantz et al.*, 2007], and the Reykjanes Ridge [*Miettinen et al*., 2012], thus supporting our findings. In contrast, a generally higher SST during the LIA (a period of climate cooling) was reported from the Labrador Sea [*Seidenkrantz et al.*, 2007],

NE Newfoundland [*Sicre et al.*, 2014], North Iceland shelf (Figure 8f) [*Justwan and Koç*, 2008], and the Reykjanes Ridge (Figure 8h) [*Andersen et al.*, 2004a; *Miettinen et al.*, 2012]. The cold-water conditions during the MCA and warm-water conditions during the LIA identified in this study support the antiphase relationship between SST in the west sector of the North Atlantic and climate trend in the NW Europe [*Krawczyk et al.*, 2010, 2013]. The antiphase identified during the MCA can be linked to the positive NAO, when a strong contrast between Icelandic Low and Azores High leads to a large ocean temperature gradient between west (i.e., low temperature) and east (i.e., high temperatures) [*Andersen et al.*, 2004a]. The relatively long-lasting, centennial-scale phases of positive NAO have been reported both for the RWP [*Olsen et al.*, 2012] and especially for the MCA [*Trouet et al.*, 2009; *Olsen et al.*, 2012]. Our April SIC along with July SST data indicate that the surface conditions were warmer in the study area during the RWP than during the MCA which is in line with a slightly weaker NAO phase during the RWP compared with that of the MCA. Also, linked with the long-lasting positive NAO phase, an enhanced Atlantic Meridional Overturning Circulation (AMOC) and northwest heat transport could have triggered coastal glacial melting in the West Greenland region during the MCA leading to the freshening of the surface water and further cooler SST and increased sea ice in the study area. The "LIA antiphase" on the other hand corresponds to a longer persisting (i.e., more numerous) negative NAO phase suggested for the late Holocene [*Andersen et al.*, 2004a; *Miettinen et al.*, 2011] and characterized by weaker contrast between the Icelandic Low and Azores High leading to weaker heat transport to the north [*Andersen et al.*, 2004a]. Also, the intensification of the subpolar gyre linked to the variability of the AMOC is suggested to explain the recorded positive SSTs resulting from increased advection of Atlantic Water (Irminger Water) by the WGC during the LIA [*Miettinen et al.*, 2012]. Intensified inflow of the Irminger Current into the SE Greenland shelf was suggested at 0.7 cal ka B.P. [*Andresen et al.*, 2013]. In addition, other studies show higher air temperatures in the West Greenland region [e.g., *Long et al.*, 2012] and change in moisture source over central Greenland suggesting a stronger meridional circulation during the LIA [e.g., *Dawson et al.*, 2003], thus supporting the positive temperature anomaly pattern identified in the western sector of the North Atlantic region (see above).

5.3. The Significance of the West Greenland Region

The dynamic nature of the climate-ocean-ice sheet interactions along the West Greenland margin make it an important region to study to improve our understanding of potential future impacts of climate change. This region has a wide range in modern-day sea ice concentration (SIC) linked to significant spatial and temporal variability in glacial-derived meltwater, as well as significant variability in ocean forcing linked to the Atlantic-sourced Irminger Water and Arctic-sourced Polar Water of the West Greenland Current (WGC). Ocean circulation within the West Greenland region is a key part of the Baffin Bay circulation system and feeds directly into the Labrador Sea, an area of importance in the global thermohaline circulation system. Changes in SIC and sea surface temperature (SST) related to meltwater flux and variability in the WGC have potential implications for deep-water formation in the Labrador Sea and the larger-scale thermohaline circulation. Reconstructing past changes in oceanographic conditions such as sea ice cover and SST, and their relationship to broader climate, oceanographic, and ice sheet trends will help to improve our understanding of the links between these important elements of the climate system. During the early Holocene, the high variability of April SIC and July SST reconstructed in this study indicates significant meltwater delivery from western Greenland Ice Sheet into the Baffin Bay region. Such meltwater delivery would potentially feed through to the Labrador Sea impacting on the formation of Labrador Sea Water, an important component of the broader Atlantic Meridional Overturning Circulation (AMOC). The reduction of significant meltwater delivery to the West Greenland margin identified here coincides with a significant change in the Labrador Sea recorded at ~7.6 cal ka B.P. indicating the start of convection at the formation of Labrador Sea Water, similar to the modern circulation system [*Gibbs et al.*, 2015]. Subsequently, the late Holocene antiphase relationship between West Greenland oceanographic conditions and general NW European conditions identified here also have the potential to influence broader oceanographic circulation and the AMOC. Even the recently observed decadal changes resulting in reduced sea ice cover and increased glacial discharge into the Baffin Bay region [e.g., *Comiso*, 2006; *Vinther et al.*, 2009] are likely to have a significant impact on the surface water density, in turn altering the strength of the AMOC [*Bakker et al.*, 2012]. Quantitative reconstructions, such as those presented here, will be useful in testing and refining future climate model outputs. It is, therefore, important to develop quantitative reconstructions of oceanographic conditions from local/regional data sets that can be directly comparable with corresponding satellite-derived data.

6. Concluding Remarks

The newly developed modern diatom data set from the West Greenland region has proven to be reliable for generating quantitative reconstructions of surface water temperature and sea ice cover in the area using a transfer function method. The advantage of our analyses over past research is that the modern data set used in our study is from the same region as the paleoreconstructions and, by restricting our surface samples to those that have a modern age based on ^{210}Pb and ^{137}Cs analyses, we eliminate any problems of reworking of surface sediments and transportation of diatoms. Our ~11,000 year high-resolution diatom record from Disko Bay revealed a clear influence of primarily spring sea ice concentration (i.e., April SIC) and also summer sea surface temperature (i.e., July SST) on changes in oceanographic conditions. Strong centennial-scale outbursts of spring time melting of sea ice and increasing temperature in summer waters prevailed during the early Holocene deglaciation of the western Greenland Ice Sheet. These conditions stabilized during the Holocene Thermal Optimum for at least 5000 years. The late Holocene antiphase relationship between surface water conditions in the Disko Bay area and climate trends in NW Europe, i.e., high April SIC during the warm Medieval Climate Anomaly and higher July SST during the cold Little Ice Age (LIA), reflect a stronger seasonality and fluctuations within the North Atlantic Oscillation. The LIA antiphase is particularly interesting as higher SSTs were recorded from a broader western sector of the North Atlantic as a possible result of variability in the Atlantic Meridional Overturning Circulation. The reconstructed April SIC supported by July SST corresponds well with the atmospheric temperature trends reconstructed from the GISP2 ice core data for the early to middle Holocene (~11.0–4.5 cal ka B.P.).

Acknowledgments

The authors wish to thank the Grønlands Forskningsråd and Greenland Institute of Natural Resources for funding the project "Sea ice during Holocene"; Søren Rysgaard and Malene Simon for supporting the project. The authors thank the Deutsche Forschungsgemeinschaft (DFG) for funding the project "Disco Climate" (MO 1422/2-1) and the Polish National Science Centre in Cracow for funding the West-East Greenland project (DEC-2011/03/N/ST10/05794). We thank the Department of Fish and Shellfish, Greenland Institute of Natural Resources and help provided by Helle Siegstad, Nanette Hammeken Arboe, Henrik Lund, and Anja Retzel during the annual survey 2014 along the West Greenland coast on board of R/V *Paamiut*. We also acknowledge helpful information provided by participants of the 2007 R/V *Maria S. Merian* cruise to western Greenland waters in the frame of "Disko Climate" project. We wish to express our gratitude to Thomas Juul-Pedersen and John Mortensen for helpful discussions on present-day phytoplankton, primary production, and oceanography off West Greenland within the Greenland Ecosystem Monitoring (GEM) Programme; Martin Blicher for advices on statistical validity of data. The results of Principal Factor Analysis and reconstructed SIC and SST data are available in the supporting information as tables; any additional data may be obtained from D.W.K. (dikr@natur.gl).

References

Alley, R. B., A. M. Agustsdottir, and P. J. Fawcett (1999), Ice-core evidence of late-Holocene reduction in North Atlantic Ocean heat transport, *Geophys. Monogr.*, *112*, 301–312.

Andersen, C., N. Koç, A. E. Jennings, and J. T. Andrews (2004a), Nonuniform response of the major surface currents in the Nordic Seas to insolation forcing: Implications for the Holocene climate variability, *Paleoceanography*, *19*, PA2003, doi:10.1029/2002PA000873.

Andersen, C., N. Koç, and M. Moros (2004b), A highly unstable Holocene climate in the subpolar North Atlantic: Evidence from diatoms, *Quat. Sci. Rev.*, *23*, 2155–2166.

Andersen, S., L. Toudal Pedersen, G. Heygster, R. Tonboe, and L. Kaleschke (2007), Intercomparison of passive microwave sea ice concentration retrievals over the high concentration Arctic sea ice, *J. Geophys. Res.*, *112*, C08004, doi:10.1029/2006JC003543.

Andresen, C. S., M. J. Hansen, M.-S. Seidenkrantz, A. E. Jennings, M. F. Knudsen, N. Nørgaard-Pedersen, N. K. Larsen, A. Kuijpers, and C. Pearce (2013), Mid- to Late-Holocene oceanographic variability on the Southeast Greenland shelf, *Holocene*, *23*(2), 167–178, doi:10.1177/0959683612460789.

Arendt, K. E., T. Juul-Pedersen, J. Mortensen, and S. Rysgaard (2013), A 5-year study of seasonal patterns in mesozooplankton community structures in a sub-Arctic fjord reveals dominance of *Microsetella norvegica* (Crustacea, Copepoda), *J. Plankton Res.*, *35*, 105–120.

Arrigo, K. R., et al. (2012), Massive phytoplankton blooms under Arctic sea ice, *Science*, *336*, 1408.

Bakker, P., C. J. Van Meerbeeck, and H. Renssen (2012), Sensitivity of the North Atlantic climate to Greenland Ice Sheet melting during the Last Interglacial, *Clim. Past*, *8*, 995–1009.

Berner, K. S., N. Koç, F. Godtliebsen, and D. Divine (2011), Holocene climate variability of the Norwegian Atlantic Current during high and low solar insolation forcing, *Paleoceanography*, *26*, PA2220, doi:10.1029/2010PA002002.

Bianchi, G. G., and I. N. McCave (1999), Holocene periodicity in North Atlantic climate and deep-ocean flow south of Iceland, *Lett. Nat.*, *397*, 515–517.

Birks, C. J. A., and N. Koç (2002), A high-resolution diatom record of late-Quaternary sea-surface temperatures and oceanographic conditions from the eastern Norwegian Sea, *Boreas*, *31*, 323–344.

Birks, H. J. B. (1995), Quantitative palaeoenvironmental reconstructions, in *Statistical Modeling of Quaternary Science Data. Technical Guide*, vol. 5, edited by D. Maddy and J. S. Brew, pp. 161–254 , Quat. Res. Assoc., Cambridge.

Birks, H. J. B. (1998), D. G. Frey and E. S. Deevey Review #1. Numerical tools in palaeolimnology-progress, potentials, and problems, *J. Paleolimnol.*, *20*, 307–332.

Boertmann, D., and A. Mosbech (2011), Eastern Baffin Bay—A strategic environmental impact assessment of hydrocarbon activities, Aarhus University, DCE – Danish Centre for Environment and Energy, pp. 270, Scientific Report from DCE – Danish Centre for Environment and Energy No. 9.

Boertmann, D., A. Mosbech, D. Schiedek, and M. Dünweber (2013), Disko West. A strategic environmental impact assessment of hydrocarbon activities, Aarhus University, DCE – Danish Centre for Environment and Energy, pp. 306, Scientific Report from DCE – Danish Centre for Environment and Energy No. 71.

Bond, G., B. Kromer, J. Beer, R. Muscheler, M. N. Evans, W. Showers, S. Hoffmann, R. Lotti-Bond, I. Hajdas, and G. Bonani (2001), Persistent solar influence on North Atlantic climate during the Holocene, *Science*, *294*, 2130–2136.

Borcard, D., P. Legendre, and P. Drapeau (1992), Partialling out the spatial component of ecological variation, *Ecology*, *73*, 1045–1055.

Bronk Ramsey, C. (2009), Bayesian analysis of radiocarbon dates, *Radiocarbon*, *51*, 337.

Buch, E. (1981), A Review of the oceanographic conditions in subarea O and 1 in the decade 1970–79, NAFO Symposium on Environmental conditions in the Northwest Atlantic during 1970–79, NAFO Scientific Council Studies no. 5.

Buch, E. (1990), A monograph on the physical oceanography of the Greenland waters, Greenland Fisheries Research Institute report, (reissued in 2000 as Danish Meteorological Institute Scientific Report 00-12, Copenhagen), pp. 405.

Casey, K. S., T. B. Brandon, P. Cornillon, and R. Evans (2010), The past, present, and future of the AVHRR Pathfinder SST program, *Oceanogr. Space*, doi:10.1007/978-90-481-8681-5_16.

Comiso, J. C. (2006), Arctic warming signals from satellite observations, *Weather*, *61*, 70–76.
Dawson, A. G., L. Elliot, P. Mayewski, P. Lockett, S. Noone, K. Hickey, T. Holt, P. Wadhams, and I. Foster (2003), Late-Holocene North Atlantic climate 'seesaws', storminess changes and Greenland Ice Sheet (GISP2) palaeoclimates, *Holocene*, *13*, 381–392.
Degerlund, M., and H. C. Eilertsen (2010), Main species characteristics of phytoplankton spring blooms in NE Atlantic and Arctic waters (68–80°N), *Estuaries Coasts*, *33*, 242–69.
Eastwood, S., K. R. Larsen, T. Lavergne, E. Neilsen, and R. T. Tonboe (2011), OSI SAF global sea ice concentration reprocessing: product user manual, version 1.3, *EUMETSAT OSI SAF (Product 0SIOSI-409)*.
Embury, O., and C. J. Merchant (2012), A reprocessing for climate of sea surface temperature from the along-track scanning radiometers: A new retrieval scheme, *Remote Sens. Environ.*, *116*, 47–61.
Fryxell, G. A. (1975), Morphology, taxonomy, and distribution of selected diatom species of Thalassiosira Cleve in the Gulf of Mexico and Antarctic waters, Dissertation, Texas A & M University, Texas.
Gibbs, O. T., S. Steinhauer, B. Fréchette, A. de Vernal, and C. Hillaire-Marcel (2015), Diachronous evolution of sea surface conditions in the Labrador Sea and Baffin Bay since the last deglaciation, *Holocene*, *25*, 1882–1987.
Giraudeau, J., M. Cremer, S. Manthé, L. Labeyrie, and G. Bond (2000), Coccolith evidence for instabilities in surface circulation south of Iceland during Holocene times, *Earth Planet. Sci. Lett.*, *179*, 257–268.
Gradinger, R. R., and M. E. M. Baumann (1991), Distribution of phytoplankton communities in relation to the large-scale hydrographical regime in the Fram Strait, *Mar. Biol.*, *111*, 311–321.
Grimm, E. (1993), *TILIA: A Pollen Program for Analysis and Display*, Illinois State Museum, Springfield, Ill.
Hammarlund, D., S. Björck, B. Buchardt, C. Isrealson, and C. T. Thomsen (2002), Rapid hydrological changes during the Holocene revealed by stable isotope records of lacustrine carbonates from Lake Igelsjön, southern Sweden, *Quat. Sci. Rev.*, *21*, 353–370.
Hanna, E., P. Huybrechts, K. Steffen, J. Cappelen, R. Huff, C. Shuman, T. Irvine-fynn, S. Wise, and M. Griffiths (2008), Increased runoff from melt from the Greenland Ice Sheet: A response to global warming, *J. Clim.*, *21*, 331–341.
Harff, J., K. Perner, and M. Moros (Eds.) 2016, Deglaciation history, coastal development, and environmental change in West Greenland during the Holocene: Results of the R/V 'Maria S. Merian' expedition $MSM_{05/03}$, *15th June to 4th July 2007*, Meereswiss. Ber., Warnemünde, 99, doi:10.12754/msr-2016-0099.
Hasle, G. R., and B. R. Heimdal (1998), The net phytoplankton from Kongsfjorden, Svalbard, July 1988, with general remarks on species composition of Arctic phytoplankton, *Polar Res.*, *17*(1), 31–52.
Hasle, G. R., and E. E. Syvertsen (1996), Marine diatoms, in *Identifying Marine Diatoms and Dinoflagellates*, edited by C. R. Tomas, pp. 5–386 , Academic Press, San Diego, Calif.
Høyer, J. L., and J. She (2007), Optimal interpolation of sea surface temperature for the North Sea and Baltic Sea, *J. Mar. Syst.*, *65*(1), 176–189.
Høyer, J. L., P. Le Borgne, and S. Eastwood (2014), A bias correction method for Arctic satellite sea surface temperature observations, *Remote Sens. Environ.*, *146*, 201–213.
Hurrel, J. W. (1995), Decadal trends in the North Atlantic Oscillation: Regional temperatures and precipitation, *Science*, *269*, 676–679.
Jennings, A. E., M. E. Walton, C. Ó. Cofaigh, A. Kilfeather, J. Ortiz, A. de Vernal, and J. A. Dowdeswell (2014), Paleoenvironments during the Younger Dryas-Early Holocene retreat of the Greenland Ice Sheet from outer Disko trough, central west Greenland, *J. Quat. Sci.*, *29*, 27–40.
Jennings, A., K. L. Knudsen, M. Hald, C. V. Hansen, and J. T. Andrews (2002), A mid-Holocene shift in Arctic sea-ice variability on the East Greenland Shelf, *Holocene*, *12*, 49–58.
Jensen, K. G. (2003), Holocene hydrographic changes in Greenland coastal waters, Dissertation, The Geological Survey of Denmark and Greenland, Denmark.
Jiang, H., M.-S. Siedenkrantz, K. L. Knudsen, and J. Eiríksson (2001), Diatom surface sediment assemblages around Iceland and their relationship to oceanic environmental variables, *Mar. Micropaleontol.*, *41*, 73–96.
Johnsen, S., D. Dahl-Jensen, N. Gundestrup, J. P. Steffensen, H. B. Clausen, H. Miller, V. Masson-Delmotte, A. E. Sveinbjörndottir, and J. White (2001), Oxygen isotope and palaeotemperatures from six Greenland ice-core stations: Camp Century, Dye-3, GRIP, GISP2, Renland and NorthGRIP, *J. Quat. Sci.*, *16*, 299–307.
Juggins, S. (2007), *C2 Version 1.5 User Guide: Software for Ecological and Palaeoecological Data Analysis and Visualisation*, pp. 73 , Newcastle University, U. K.
Justwan, A., and N. Koç (2008), A diatom based transfer function for reconstructing sea ice concentrations in the North Atlantic, *Mar. Micropal.*, *66*, 264–278.
Juul-Pedersen, T., K. E. Arendt, J. Mortensen, D. Krawczyk, S. Rysgaard, A. Retzel, et al. (2014), Nuuk Basic: The MarineBasis programme, in *Nuuk Ecological Research Operations*, *7th Annual Report*, *2013*, edited by L. M. Jensen and M. Rasch, pp. 46–68 , National Environmental Research Institute, Aarhus University, Denmark.
Juul-Pedersen, T., K. E. Arendt, J. Mortensen, M. E. Blicher, D. H. Søgaard, and S. Rysgaard (2015), Seasonal and interannual phytoplankton production in a sub-arctic tidewater outlet glacier fjord, SW Greenland, *Mar. Ecol. Prog. Ser.*, *524*, 27–38, doi:10.3354/meps11174.
Kaufman, D. S., et al. (2003), Holocene thermal maximum in the western Arctic (0–180°W), *Quat. Sci. Rev.*, *529–560*.
Kaufman, D. S., et al. (2009), Recent warming reverses long-term Arctic cooling, *Science*, *325*, 1236–1239.
Koç Karpuz, N., and E. Jansen (1992), A high-resolution diatom record of the last deglaciation from NE Norwegian Sea: Documentation of rapid climatic changes, *Paleoceanography*, *7*, 499–520, doi:10.1029/92PA01651.
Krawczyk, D., A. Witkowski, M. Moros, J. Lloyd, A. Kuijpers, and A. Kierzek (2010), Late-Holocene diatom inferred reconstruction of temperature variations of the West Greenland Current from Disko Bugt, central West Greenland, *Holocene*, *20*(5), 659–666.
Krawczyk, D., A. Witkowski, J. Lloyd, M. Moros, J. Harff, and A. Kuijpers (2013), Late-Holocene diatom derived seasonal variability in hydrological conditions off Disko Bay, West Greenland, *Quat. Sci. Rev.*, *67*, 93–104.
Krawczyk, D., A. Witkowski, J. J. Waniek, M. Wroniecki, and J. Harff (2014), Description of diatoms from the Southwest to West Greenland coastal and open marine waters, *Polar Biol.*, *37*, 1589–1606.
Krawczyk, D., A. Witkowski, T. Juul-Pedersen, K. E. Arendt, J. Mortensen, and S. Rysgaard (2015), Microplankton succession in a SW Greenland tidewater glacial fjord influenced by coastal inflows and run-off from the Greenland Ice Sheet, *Polar Biol.*, *38*, 1515–1533.
Kullman, L. (1999), Early Holocene tree growth at a high elevation site in the northernmost Scandes of Sweden (Lapland): A palaeobiogeographical case study based on megafossil evidence, *Geogr. Ann.*, *81*, 63–74.
Lloyd, J. M. (2006), Late Holocene environmental change in Disko Bugt, west Greenland: Interaction between climate, ocean circulation and Jakobshavn Isbrae, *Boreas*, *35*, 35–49.
Lloyd, J. M., L. A. Park, A. Kuijpers, and M. Moros (2005), Early Holocene palaeoceanography and deglacial chronology of Disko Bugt, West Greenland, *Quat. Sci. Rev.*, *24*, 1741–1755.

Lloyd, J. M., M. Moros, K. Perner, R. J. Telford, A. Kuijpers, E. Jansen, and D. McCarthy (2011), A 100 yr record of ocean temperature control on the stability of Jakobshavn Isbrae, West Greenland, *Geology*, *39*, 867–870, doi:10.1130/G32076.1.

Long, A. J., S. A. Woodroffe, G. A. Milne, C. L. Bryant, M. J. R. Simpson, and L. M. Wake (2012), Relative sea-level change in Greenland during the last 700 yrs and ice sheet response to the Little Ice Age, *Earth Planet. Sci. Lett.*, *315–316*, 76–85.

Mann, M. E., Z. Zhang, S. Rutherford, R. S. Bradley, M. K. Hughes, D. Shindell, C. Ammann, G. Faluvegi, and F. Ni (2009), Global signatures and dynamical origins of the Little Ice Age and Medieval Climate Anomaly, *Science*, *326*, 1256–1260.

McGregor, H. V., et al. (2015), Robust global ocean cooling trend for the preindustrial Common Era, *Nat. Geosci.*, *8*, 671–677.

Metzeltin, D., and A. Witkowski (1996), *Diatomeen der Bären Insel. Süßwasser und marine Arten, Iconographia Diatomologica 4*, Koeltz Scientific Books, Königstein, Germany.

Miettinen, A., N. Koç, I. R. Hall, F. Godtliebsen, and D. Divine (2011), North Atlantic sea surface temperatures and their relation to the North Atlantic Oscillation during the last 230 years, *Clim. Dyn.*, *36*, 533–543, doi:10.1007/s00382-010-0791-5.

Miettinen, A., D. Divine, N. Koç, F. Godtliebsen, and I.R. Hall (2012), Multicentennial variability of the sea surface temperature gradient across the Subpolar North Atlantic over the last 2.8 kyr, *J. Clim.*, *25*, 4205–4219, doi:10.1175/JCLI-D-11-00581.1.

Miettinen, A., D. Divine, K. Husum, N. Koç, and A. Jennings (2015), Exceptional ocean surface conditions on the SE Greenland shelf during the Medieval Climate Anomaly, *Paleoceanography*, *30*, 1675–1674, doi:10.1002/2015PA002849.

Moros, M., K. Emeis, B. Risebrobakken, I. Snowball, A. Kuijpers, J. McManus, and E. Jansen (2004), Sea surface temperatures and ice rafting in the Holocene North Atlantic: Climate influences on northern Europe and Greenland, *Quat. Sci. Rev.*, *23*, 2113–2126.

Moros, M., K. G. Jensen, and A. Kuijpers (2006), Mid to Late Holocene hydrological and climate variability in Disko Bugt, central West Greenland, *Holocene*, *16*, 357–367.

Moros, M., E. Jansen, D. W. Oppo, J. Girardeau, and A. Kuijpers (2012), Reconstruction of the late-Holocene changes in the Sub-Arctic Front position at the Reykjanes Ridge, north Atlantic, *Holocene*, *22*(8), 877–886, doi:10.1177/0959683611434224.

Moros, M., et al. (2016), Surface and sub-surface multi-proxy reconstruction of middle to late Holocene palaeoceanographic changes in Disko Bugt, West Greenland, *Quat. Sci. Rev.*, *132*, 146–160.

O'Brien, S. R., P. A. Mayewski, L. D. Meeker, D. A. Meese, M. S. Twickler, and S. I. Whitlow (1995), Complexity of Holocene climate as reconstructed from a Greenland ice core, *Science*, *270*, 1962–1964.

Olsen, J., N. J. Anderson, and M. F. Knudsen (2012), Variability of the North Atlantic Oscillation over the past 5,200 years, *Nat. Geosci.*, *5*, 808–812.

Pearce, C., M.-S. Seidenkrantz, A. Kuijpers, and N. F. Reynisson (2014), A multi-proxy reconstruction of oceanographic conditions around the Younger Dryas-Holocene transition in Placentia Bay, Newfoundland, *Mar. Micropal.*, *112*, 39–49.

Perner, K., M. Moros, J. M. Lloyd, A. Kuijpers, R. J. Telford, and J. Harff (2011), Centennial scale benthic foraminiferal record of late Holocene oceanographic variability in Disko Bugt, West Greenland, *Quat. Sci. Rev.*, *30*, 2815–2826.

Perner, K., M. Moros, A. Jennings, J. M. Lloyd, and K. L. Knudsen (2013), Holocene palaeoceanographic evolution off West Greenland, *Holocene*, *23*, 374–387.

Quillfeldt, C. H. (1996), Ice algae and phytoplankton in north Norwegian and arctic waters: Species composition, succession and distribution, Dissertation, University of Tromsø, Norges fiskerihøgskole, Norway.

Quillfeldt, C. H. (2001), Identification of some easily confused common diatom species in Arctic spring blooms, *Bot. Mar.*, *44*, 375–389.

Reimer, P. J., et al. (2009), IntCal09 and Marine09 radiocarbon age calibration curves, 0–50,000 years cal BP, *Radiocarbon*, *51*, 1111–1150.

Ren, J., H. Jiang, M.-S. Seidenkrantz, and A. Kuijpers (2009), A diatom-based reconstruction of Early Holocene hydrographic and climatic change in a southwest Greenland fjord, *Mar. Micropaleontol.*, *70*, 166–176.

Ribeiro, S., M. Moros, M. Ellegaard, and A. Kuijpers (2012), Climate variability in West Greenland during the last 1500 years—Evidence from a high-resolution marine palynological record from Disko Bay, *Boreas*, *41*, 68–83.

Ribergaard, M. H. (2014), Oceanographic Investigations off West Greenland 2013, NAFO Scientific Council Documents, Dartmouth, Nova Scotia, Canada.

Ribergaard, M. H., S. A. Pedersen, B. Aadlandsvik, and N. Kliem (2004), Modelling the ocean circulation on the West Greenland shelf with special emphasis on northern shrimp recruitment, *Cont. Shelf Res.*, *24*, 1505–1519.

Roberts, D. H., A. J. Long, C. Schnabel, B. J. Davies, S. Xu, M. J. R. Simpson, and P. Huybrechts (2009), Ice sheet extent and early deglacial history of the southwestern sector of the Greenland Ice Sheet, *Quat. Sci. Rev.*, *28*, 2760–2773.

Roncaglia, L., and A. Kuijpers (2004), Palynofacies analysis and organic-walled dinoflagellate cysts in late-Holocene sediments from Igaliku Fjord, South Greenland, *Holocene*, *14*(2), 172–184.

Schrader, H. J., and R. Gersonde (1978), Diatoms and silicoflagellates, in *Micropaleontological Counting Methods and Techniques and Exercise on an Eight Meters Section of the Lower Pliocene of Capo Rosello, Silicy*, vol. 17, edited by W. J. Zachariasse et al., pp. 129–176, Utrecht Micropaleontological Bulletins, Netherlands.

Seidenkrantz, M.-S., S. Aagaard-Sørensen, H. Sulsbrück, A. Kuijpers, K. G. Jensen, and H. Kunzendorf (2007), Hydrography and climate of the last 4400 years in a SW Greenland fjord: Implications for Labrador Sea palaeoceanography, *Holocene*, *17*, 387–401.

Seidenkrantz, M.-S., L. Roncaglia, A. Fischel, C. Heilmann-Clausen, A. Kuijpers, and M. Moros (2008), Variable North Atlantic climate seesaw patterns documented by a late Holocene marine record from Disko Bugt, West Greenland, *Mar. Micropal.*, *68*(1–2), 66–83.

Seidenkrantz, M.-S., H. Ebbesen, S. Aagaard-Sørensen, M. Moros, J. Lloyd, J. Olsen, M. F. Knudsen, and A. Kuijpers (2013), Early Holocene large-scale meltwater discharge from Greenland documented by foraminifera and sediment parameters, *Palaeogeogr. Palaeoclimatol. Palaeoecol.*, *391*, 71–81.

Sha, L., H. Jiang, and K. L. Knudsen (2012), Diatom evidence of climatic change in Holsteinsborg Dyb, west of Greenland, during the last 1200 years, *Holocene*, *22*, 347–358.

Sha, L., H. Jiang, M.-S. Seidenkrantz, K. L. Knudsen, J. Olsen, A. Kuijpers, and Y. Liu (2014), A diatom-based sea-ice reconstruction for the Vaigat Strait (Disko Bugt, West Greenland) over the las 5000 yr, *Palaeogeogr. Palaeoclimatol. Palaeoecol.*, *403*, 66–79.

Sheldon, C., A. Jennings, J. T. Andrews, C. Cofaigh, K. Hogan, J. A. Dowdeswell, and M.-S. Seidenkrantz (2016), Ice stream retreat following the LGM and onset of the West Greenland Current in Uummannaq Trough, West Greenland, *Quat. Sci. Rev.*, doi:10.1016/j.quascirev.2016.01.019.

Sicre, M.-A., et al. (2014), Labrador current variability over the last 200 years, *Earth Planet. Sci. Lett.*, *400*, 26–32.

Snowball, I., P. Sandgren, and G. Pettersen (1999), The mineral magnetic properties of an annually laminated Holocene lake-sediment sequence in northern Sweden, *Holocene*, *9*, 353–362.

Söderkvist, J., T. G. Nielsen, and M. Jespersen (2006), Physical and biological oceanography in West Greenland waters with emphasis on shrimp and fish larvae distribution, pp. 60, National Environmental Research Institute (NERI), University of Aarhus, Denmark, NERI Technical Report No. 581.

Stötter, J., M. Wastl, C. Caseldine, and T. Häberle (1999), Holocene palaeoclimatic reconstruction in northern Iceland: Approaches and results, *Quat. Sci. Rev.*, *18*, 457–474.

Syvertsen, E. E. (1979), Resting spore formation in clonal cultures of *Thalassiosira antarctica* Comber, *T. nordenskioeldii* Cleve and *Detonula confervacea* (Cleve) Gran, *Nova Hedwigia*, *64*, 4–63.

Tang, C. C., C. K. Ross, T. Yao, B. Petrie, B. M. DeTracey, and E. Dunlap (2004), The circulation, water masses and sea-ice of Baffin Bay, *Prog. Oceanogr.*, *63*, 183–228.

ter Braak, C. J. F., and S. Juggins (1993), Weighted averaging partial least squares regression (WA-PLS): An improved method for reconstructing environmental variables from species assemblages, *Hydrobiologia*, *269*/270, 485–502.

Throndsen, J., G. R. Hasle, and K. Tangen (2003), *Norsk Krystplanktonflora*, Almater Forlag As, Oslo, Norway.

Tonboe, R., R.-H. Pfeiffer, and M. B. Jensen (2015), Validation report for Global sea ice concentration reprocessing, *Products OSI-409*, *Osi-409a*, *OSI-430. V. 2.0*, pp. 30.

Trouet, V., J. Esper, N. E. Graham, A. Baker, J. D. Scourse, and D. C. Frank (2009), Persistent positive North Atlantic Oscillation mode dominated the Medieval Climate Anomaly, *Science*, *324*, 78–80.

Upton, G., and I. Cook (2002), *The Oxford Dictionary of Statistics*, pp. 420, Oxford Univ. Press, New York.

Vinther, B. M., et al. (2009), Holocene thinning of the Greenland ice sheet, *Nature*, *461*(17), 385–388, doi:10.1038/nature08355.

Weckström, K., A. Miettinen, B. Caissie, C. Pearce, M. Ellegaard, D. Krawczyk, and A. Witkowski (2014), Sea surface temperatures in Disko Bay during the Little Ice Age—Caution needs to be exercised before assigning *Thalassiosira kushirensis* resting spores as a warm-water indicator in palaeoceanographic studies, *Quat. Sci. Rev.*, *101*, 234–237.

Williams, K. M., J. T. Andrews, N. J. Weiner, and P. J. Mudie (1995), Late Quaternary Paleoceanography of the mid- to outer continental shelf, east Greenland, *Arctic Alpine Res.*, *27*, 352–363.

Witak, M., A. Wachnicka, A. Kuijpers, S. Troelstra, M. A. Prins, and A. Witkowski (2005), Holocene North Atlantic surface circulation and climatic variability: Evidence from diatom records, *Holocene*, *15*(1), 85–96.

Witkowski, A., H. Lange-Bertalot, and D. Metzeltin (2000), *Diatom Flora of Marine Coasts I, Iconographia Diatomologica 7*, Koeltz Scientific Books, Königstein, Germany.

Young, N. E., and J. P. Briner (2015), Holocene evolution of the western Greenland Ice Sheet: Assessing geophysical ice-sheet models with geological reconstructions of ice-margin change, *Quat. Sci. Rev.*, *114*, 1–17.